The Meteoritical Society

Meteoritics & Planetary Science 47, Nr 1, 99–119 (2012)
doi: 10.1111/j.1945-5100.2011.01315.x

The effects of disk building on the distributions of refractory materials in the solar nebula

Le YANG* and Fred J. CIESLA

Department of the Geophysical Sciences, The University of Chicago, Chicago, Illinois 60637, USA
*Corresponding author. E-mail: leyang@uchicago.edu

(Received 23 May 2011; revision accepted 02 November 2011)

Abstract–Refractory materials, such as calcium-aluminum-rich inclusions (CAIs) and crystalline silicates, are widely found in chondritic meteorites as well as comets, taken as evidence for large-scale mixing in the solar nebula. Most models for mixing in the solar nebula begin with a well-formed protoplanetary disk. Here, we relax this assumption by modeling the formation and evolution of the solar nebula during and after the period when it accreted material from its parent molecular cloud. We consider how disk building impacts the long-term evolution of the disk and the implications for grain transport and mixing within it. Our model shows that materials that formed before infall was complete could be preserved in primitive bodies, especially those that accreted in the outer disk. This potentially explains the discovery of refractory objects with low initial $^{26}Al/^{27}Al$ ratios in comets. Our model also shows that the highest fraction of refractory materials in meteorites formed around the time that infall stopped. Thus, we suggest that the calcium-aluminum-rich inclusions in chondrites would be dominated by the population that formed during the transition from class I to class II stage of young stellar objects. This helps us to understand the meaning of $t = 0$ in solar system chronology. Moreover, our model offers a possible explanation for the existence of isotopic variations observed among refractory materials—that the anomalous materials formed before the collapse of the parent molecular cloud was complete.

INTRODUCTION

Studies of chondritic meteorites and cometary materials demonstrate that mixing and transport in the solar nebula played critical roles in defining the properties of those primitive bodies. Calcium-aluminum-rich inclusions (CAIs), which are common components of chondritic meteorites, were found in the materials collected from comet Wild 2 by the Stardust spacecraft (Brownlee et al. 2006). This was surprising because CAIs or their precursors are aggregates of minerals which are thought to have condensed out of a solar composition gas during cooling from very high temperature $> \sim$1300–1700 K (Grossman 1972, 2010), whereas the comet is believed to come from the cold outer region of the disk where temperatures of approximately 10–50 K are expected. High-temperature grains have also been identified spectroscopically in comets (Harker et al. 2002, 2004a, 2004b; Lisse et al. 2006) with surprisingly high mass fractions of Mg-rich silicate crystals given that crystalline silicates are essentially absent from the interstellar medium (Kemper et al. 2004). As the CAIs and crystalline grains returned by Stardust are isotopically similar to those found in chondritic meteorites (McKeegan et al. 2006), the high-temperature materials found in comets are now thought to have formed in the hot, inner regions of our protoplanetary disk and then were transported outwards to be made available for comets. Thus, understanding how and when materials were transported and mixed in the solar nebula is necessary to fully develop our understanding of solar system evolution.

A number of mechanisms have been proposed as being responsible for the transport of materials in the solar nebula. Among them is the idea that solid particles and gas molecules would be redistributed during the dynamical evolution of the disk. Most of the gas in the disk moved inwards and was ultimately accreted by

the young Sun, whereas some gas was transported outwards by viscous stresses to conserve angular momentum (Shakura and Sunyaev 1973; Lynden-Bell and Pringle 1974; Nakamoto and Nakagawa 1994). Small dust particles coupled to the gas would have been subjected to these motions, moving inward or outward along with the gas in which they were suspended. They would have also been subjected to diffusion from turbulence, if present, and experienced random motions which resulted in them being redistributed, generally from high concentrations to low ones.

Large particles—those with stopping times comparable to the orbital period of the gas—would have begun to decouple from the gas (Weidenschilling 1977). The gas orbited the central star with sub-Keplerian velocity due to the outward pressure gradient in the disk, whereas those particles, which would have otherwise orbited at Keplerian velocity, drifted inward as they lost energy and angular momentum when they interacted with the gas. The inward velocity of solids was a strong function of their size. Millimeter- to centimeter-size particles, such as CAIs found in CV chondrites (MacPherson 2005), would have drifted inward hundreds of AU in the Minimum Mass Solar Nebula within 1 Myr, or be lost to the Sun on shorter time scales. Given the 1–3 Myr age difference between these CAIs and chondrules (Amelin et al. 2002, 2010; Scott 2007; Krot et al. 2009), those CAIs must have had their inward drift motions offset in some way, such as moving with outward gas flow associated with mass and angular momentum transport within the disk (Cuzzi et al. 2003; Ciesla 2010; Jacquet et al. 2011).

Cuzzi et al. (2003) studied the formation and redistribution of CV-like CAIs (1–5 mm in radius) in a viscously evolving solar nebula, and found that some can survive in the disk for more than 1 Myr, as the large-scale outward expansion and the turbulent diffusion associated with disk evolution can overcome the inward motions associated with gas drag. Ciesla (2010) modeled the redistributions of high-temperature materials formed at different times within an evolving solar nebula and found that the most abundant refractory objects which were preserved within the solar nebula were those that formed in the first approximately 10^5 yr of solar nebula evolution. This is because, first, the disk was hottest and contained the largest amount of mass at this early epoch, allowing greater amounts of high-temperature materials to form than any other subsequent period. Second, those high-temperature materials that formed earliest could get carried outward during the radial expansion of the disk as mass and angular momentum were transported most rapidly during this period. At later times, the region where CAIs would have formed was located very close to the Sun whereas the location where the net gas motions were directed outwards was located much farther out in the disk. Thus, those later formed high-temperature objects were less efficiently preserved. As such, Ciesla (2010) argued that due to the dynamics of those high-temperature products in the disk, CAIs would exhibit a small spread in formation ages, which was consistent with the observed ages of CAIs found in CV chondrites (Thrane et al. 2006; Jacobsen et al. 2008). Further, as these objects define our time zero in the chronology of the solar system, Ciesla (2010) concluded that this time corresponded to the point where the solar nebula was most massive, which would roughly be the transition phase from a class I to class II source in terms of the classification of young stellar objects (Lada and Wilking 1984; Lada and Shu 1990). That means that the preserved CAIs were dominated by materials that formed right at the time when the disk stopped accreting mass from its parent cloud core.

Here, we build on the model of Ciesla (2010) to understand the origin of high-temperature materials and how they were mixed throughout the solar system. A common assumption in solar nebula evolution models, as well as most others which study the transport of materials in the solar nebula, is that the disk fully formed before transport began—that is, the disk had ceased accreting materials from its parent cloud core. Here, we relax that assumption by modeling the formation and evolution of the Sun and solar nebula beginning with the collapse of the parent molecular cloud core. We explore how high-temperature materials formed at different epochs would have been redistributed through the disk. This allows us to explore whether the results of Ciesla (2010) hold and to what extent comets and primitive asteroids may preserve a record of the collapse phase of the cloud that formed our solar nebula.

In the following section, we present the model used here that describes the formation and evolution of the solar nebula, and transport of materials within it. We then discuss in detail the results of a single model run to show how solids are formed and transported in the physical context adopted here. Following that discussion, we explore how changes in key parameters affect the results of the model. We end with our main conclusions and discuss the implications that our results have for interpreting data from meteoritic and cometary materials.

MODEL DESCRIPTION

Model Overview

Young stars and their protoplanetary disks form as a result of the gravitational collapse of a molecular cloud core. While some of the mass in the cloud is

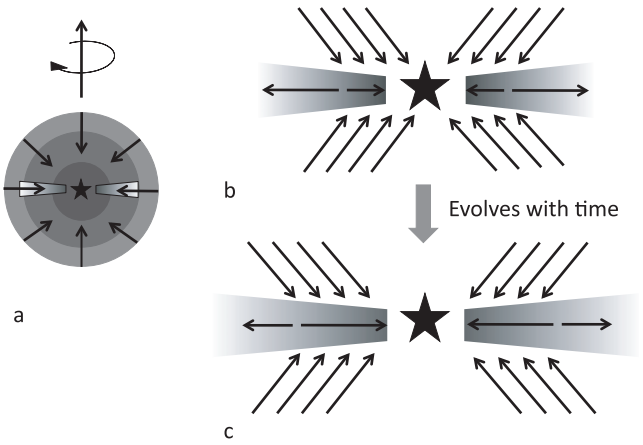

Fig. 1. A diagram of the stages of formation considered here. In (a), the proto-sun and disk form within a rotating molecular cloud. In (b) the disk has just begun to form as mass is incorporated from the molecular cloud at distances that are very close to the star, while (c) shows that material is added to the disk later on, but over a greater radial extent. As the disk evolves, it expands in space. The black arrows in (b) and (c) indicate the net movement of materials within the disk. The direction of each arrow represents the direction of transport, and the length of each arrow is proportional to the amount of material transported in each direction.

accreted directly by the central protostar, the rest settles into a disk that orbits the protostar as a result of angular momentum conservation (Lynden-Bell and Pringle 1974). The disk also feeds mass to the central star through internal dissipation processes that drive mass inwards and angular momentum outwards, as illustrated in Fig. 1. This dissipation operates even after the collapse stage stopped, and the central star continues to accrete mass from the disk. The transport of mass through the disk also determines the thermal environments within which planetary materials are processed. The disk is generally hotter throughout at early stages due to the greater rates of internal dissipation, and cools over time as the rate of dissipation slows and radiation escapes more readily. Here, we aim to understand how each of these stages of evolution impacted the properties of the refractory objects that formed, with particular attention on those that remained in the solar nebula for millions of years. We largely follow the model of Hueso and Guillot (2005) in describing the physical growth and evolution of the disk. We note that this model has also been adopted in studies of the early evolution of protoplanetary disks (e.g., Dullemond et al. 2006; Zhu et al. 2010). In the following subsections, we describe the details of the model. After that we present our results, and describe how each physical process we consider impacts the results of our calculations.

Cloud Core Collapse

In our model, the presolar cloud is taken, for the sake of simplicity, as an isothermal and spherically symmetric envelope. We adopt the picture developed by Shu (1977) showing that the molecular cloud undergoes inside-out collapse with the mass accretion rate from the envelope to the disk being:

$$\dot{M} = 0.975\frac{c_s^3}{G}. \quad (1)$$

Here G is gravitational constant and c_s is the cloud local sound speed in the cloud where $c_s = ((\gamma k T_{cd})/\bar{m})^{1/2}$, with γ being the gas adiabatic index and taken as 1.4, appropriate for a gas dominated by molecular hydrogen; k is Boltzmann's constant; and $\bar{m}$ is the mean molecular weight of the predominately H_2 gas. The temperature of the cloud, T_{cd}, is a free parameter in our model. Typical temperatures of such clouds fall between 10 and 20 K (Van Dishoeck et al. 1993). In this model, the rate of material falling from the isothermal cloud into the solar system is a constant throughout the entire infall stage.

Where infalling material is accreted in the disk depends on its specific angular momentum. That is, the material in a given cylindrical shell of radius r in the cloud collapses onto the disk within a centrifugal radius R_c, which is defined by equating the angular momentum of the material in the shell to that of the material when it was incorporated into the disk. With the assumption that the presolar cloud rotates rigidly with a constant angular velocity, the centrifugal radius can be parameterized by (Hueso and Guillot 2005)

$$R_c(t) \approx 53\left(\frac{\omega_{cd}}{10^{-14}\mathrm{s}^{-1}}\right)^2\left(\frac{T_{cd}}{10\mathrm{K}}\right)^{-4}\left(\frac{M(t)}{1M_\odot}\right)^3, \quad (2)$$

where ω_{cd} is the cloud's initial angular velocity and is a free parameter in our simulations. Typical values of ω_{cd} are estimated to range from 10^{-15} to 10^{-13} s^{-1} based on observed velocity gradients in the cloud (Goodman et al. 1993; Barranco and Goodman 1998; Lodato 2008). $M(t)$ is the total mass of the star–disk system at time t. The distribution of materials falling into the disk within the centrifugal radius as determined by angular momentum balance is expressed as

$$S(R,t) = \frac{\dot{M}}{8\pi R_c^2}\left(\frac{R}{R_c}\right)^{-3/2}\left[1-\left(\frac{R}{R_c}\right)^{1/2}\right]^{-1/2}. \quad (3)$$

Disk Evolution

The evolution of disk materials is modeled by adopting the classical α-viscosity formalism (Shakura

and Sunyaev 1973; Lynden-Bell and Pringle 1974; Hartmann et al. 1998). We assume a thin and axisymmetric disk, such that we can focus on how the surface density evolves as a function of distance from the Sun. The equations describing the evolution of the surface density in the infall stage are

$$\begin{aligned} \frac{\partial \Sigma}{\partial t} + \frac{1}{R}\left(\frac{\partial R\Sigma v_r}{\partial R}\right) &= S(R,t), \quad \text{if } R \le R_c(t), \\ \frac{\partial \Sigma}{\partial t} + \frac{1}{R}\left(\frac{\partial R\Sigma v_r}{\partial R}\right) &= 0, \quad \text{if } R > R_c(t) \end{aligned} \tag{4}$$

where $S(R,t)$ is the source term given in Equation 3. After infall stopped, the source term is zero throughout the disk. The net radial velocity of gas, v_r, is given by $v_r = -(3/\Sigma\sqrt{R})(\partial/\partial R)(\Sigma\nu\sqrt{R})$ where ν is the local viscosity of the disk. In our simulations, the viscosity is described by the α-prescription $\nu = \alpha \cdot Cs \cdot H$, (Shakura and Sunyaev 1973). Cs is the local sound speed, which is calculated by $Cs = (\gamma k T_m/\bar{m})^{1/2}$, with T_m as the local temperature in the midplane. The scale height, H, equals to the ratio of the local sound speed over the angular velocity at that position in the disk, $H = Cs/\Omega$, with Ω being the local Keplerian frequency. We discuss our choices of α further below.

The thermal evolution of the disk is calculated by balancing the heat input with the cooling rate. In our simulation, the disk is heated by viscous dissipation, irradiation from the central star, and radiation from the cloud envelope, while the disk cools as energy is lost by radiation from the disk surface. Mathematically, the balance of these effects is given by:

$$2\sigma T_e(R,t)^4 = \frac{9}{4}\Sigma\nu\Omega^2 + 2\sigma T_{cd}^4 + 2\sigma T_{irr}^4, \tag{5}$$

where σ is the Stefan–Boltzmann constant. The effective temperature of the disk surface, T_e, determines the rate of energy lost from the disk. The first term on the right side of the above equation represents the heat produced by viscous dissipation. The second term is the radiation from the ambient cloud envelope. The third term corresponds to the irradiation from the central star, where the T_{irr} is

$$T_{irr} = T_\odot \left[\frac{2}{3\pi}\left(\frac{R_\odot}{R}\right)^3 + \frac{1}{2}\left(\frac{R_\odot}{R}\right)^2 \frac{H}{R}\left(\frac{d\ln H}{d\ln R} - 1\right)\right]^{1/4}. \tag{6}$$

Here, $T_\odot$ is the central star's surface temperature, and taken to be 4000 K. $R_\odot$ is radius of the central star, and is 0.01 AU in our simulations. The first term inside the brackets describes irradiation from the central star to a flat disk, and the second term accounts for the flaring of the disk (Adams et al. 1988; Ruden and Pollack 1991).

While the above equation gives us information on the effective temperature of the disk at its surface, for planetary materials we are more concerned with the temperatures at the disk midplane. If we assume that all dissipated energy is released at the disk midplane, then the diffusion of radiation to the disk surface implies (Armitage et al. 2001):

$$T_m(R,t)^4 = \frac{3}{4}\tau T_e(R,t)^4. \tag{7}$$

Here, τ is the optical depth, and is given by $\tau = (\kappa\Sigma)/2$, where κ is the opacity of gas and dust of the disk. While the exact value for κ depends on the local pressure and temperature in the disk (Pollack et al. 1985), a gas with solar composition at the temperatures expected in the solar nebula will have a value of approximately 1–5 $cm^2\ g^{-1}$ (Cassen 2001).

Material Transport in the Disk

Materials suspended within the disk are passively transported along with the gas and also are subject to radial diffusion (Dullemond et al. 2006). These processes are described by:

$$\frac{\partial \Sigma_i}{\partial t} + \frac{1}{R}\frac{\partial R\Sigma_i v_r}{\partial R} = \frac{1}{R}\frac{\partial}{\partial R}\left[RD\Sigma\frac{\partial}{\partial R}\left(\frac{\Sigma_i}{\Sigma}\right)\right] + S_i(R,t), \tag{8}$$

where Σ_i is the surface density of material that we are looking at, and the subscript i refers to different material populations. D is the diffusion coefficient and $S_i(R,t)$ is the source term of materials that are added from infall or heated in the disk. We assume a constant gas-to-dust ratio in that infalling material. In the case of silicate dust, the ratio would be 200, which is within the typical range for molecular clouds (Young and Scoville 1991), and roughly the ratio expected in equilibrium condensation models for the solar nebula (Lodders 2003).

The first term on the right hand side of Equation 8 describes the diffusive redistribution of materials. Here, we make the typical, first-order assumption that $D = \nu$, where ν is the viscosity. In the absence of diffusion, the equation above is exactly the same as Equation 4, except for the solids instead of the gas. This is only valid for particles that are small enough to be perfectly coupled to the gas, and works for most CAIs that are smaller than millimeter size. However, for some CAIs in the CV3 chondrites, they are in the millimeter- to centimeter-size range, and would be affected by gas drag. As such, the radial velocity and diffusivity would be slightly changed, an issue we return to in the Variations of Grain Size section.

Table 1. Parameters used in our study.

Parameters	Typical values	Values in the standard model *a*	Other models considered
ω_{cd}	10^{-14}–10^{-13} s^{-1} [1]	10^{-14} s^{-1}	Model *b*: 5×10^{-15} s^{-1} Model *c*: 2×10^{-14} s^{-1}
T_{cd}	10–20 K [2]	15 K	Model *d*: 10 K Model *e*: 20 K
α	10^{-5}–0.1 [3]	10^{-3}	Model *f*: 10^{-5} Model *g*: varies from 10^{-5} to 10^{-2}
κ	1–5 cm^2 g^{-1} [4]	1 cm^2 g^{-1}	Model *h*: varies with *T*

Note: [1] Goodman et al. (1993) and Lodato (2008); [2] Van Dishoeck et al. (1993); [3] Hartmann et al. (1998) and Hueso and Guillot (2005); [4] Cassen (2001).

Numerical Approach

We begin our simulation with a central star that is 0.05 $M_\odot$ embedded in a collapsing molecular cloud core. Those equations describing the $\Sigma(R, t)$ evolution are solved numerically using an explicit finite-difference scheme on a computational grid for the disk that is made of 150 annuli. The first annulus is centered on 0.05 AU. The radial distance between the n + 1st and nth annulus is $1.1^n \times 0.1$ AU. Any mass pushed inward into the first grid is assumed to be added to the Sun, and thus removed from the disk. Equations describing local conditions in the disk are then solved during each timestep to give the local and physical conditions everywhere in the disk.

NUMERICAL RESULTS AND APPLICATIONS

Solar Nebula Evolution

In this section, we present the results of what we define as our standard case (model *a* in Table 1). In this model, we set the angular velocity of the 1 $M_\odot$ parent cloud core, ω_{cd}, as 10^{-14} s^{-1}, and the temperature T_{cd} as 15 K. This gives a mass accretion rate from the cloud core to the star–disk system of 3.17×10^{-6} $M_\odot$ yr^{-1}, meaning infall ends at approximately 0.3 Myr. The opacity, K, is set to 1 cm^2 g^{-1} everywhere.

The turbulent viscous parameter, α, within a protoplanetary disk is uncertain, with estimates ranging from essentially zero to approximately 0.1 (Hartmann et al. 1998; Hueso and Guillot 2005). While α may not be constant in space in time, we assume a uniform value of 0.001 in the standard model. We allow this value to be augmented in gravitationally unstable regions by locally increasing it by an amount $0.01((Q_{crit}^2/Q^2) - 1)$ (Armitage et al. 2001) in the region where Q is smaller than some critical value Q_{crit}. Here, Q, given by $(Cs\Omega)/(\pi G\Sigma)$ (Toomre 1964), quantifies the strength of self-gravity in the disk. We adopt $Q_{crit} = 2$, as this generally represents the condition where self-gravity exceeds the tidal force exerted by the central star and spiral arms become effective in driving large-scale motions (Armitage et al. 2001; Boss 2004, 2008).

The left panel of Fig. 2 shows how the star mass, disk mass, and total mass of the star–disk system evolve with time, whereas the right panel shows how the centrifugal radius, which is the outermost location where mass is added to the star–disk system from the parent cloud, grows with time. The inner edge of the disk is set to be 0.1 AU. As such, no material is added to the disk until about 0.05 Myr, as the centrifugal radius moves beyond 0.1 AU at this time. Prior to this, all mass is added directly to the star. Once the centrifugal radius grows beyond the inner edge of the disk, material is then added to both the star and the disk, leading each to grow more massive with time. In addition, the material in the disk is redistributed due to viscous stresses, causing some mass to be accreted from the disk onto the star.

At 0.3 Myr, all of the 1 $M_\odot$ molecular cloud material has been incorporated into the star–disk system, and infall stops. During subsequent evolution, the disk decreases in mass as materials are continuously pushed through its inner edge and accreted onto the star. This process lasts for millions of years. Note that after 3 Myr of evolution, the star reaches only approximately 0.9 $M_\odot$ in this case.

Figure 3 shows the disk surface density, Σ, and disk midplane temperature, T_m, at various times over the course of the evolution described above. The surface density near the star increases with time early on as mass is added to the disk during the first 0.3 Myr. All of the mass falls inside of the centrifugal radius shown in Fig. 2, which reaches a maximum of 10 AU at the final stages of infall. Mass found outside of the centrifugal radius at any point of disk evolution is because it was pushed outward to that distance as a consequence of the disk viscous spreading associated with angular momentum conservation. That is, all materials located outside of 10 AU originally were located closer to the Sun, earlier in disk history.

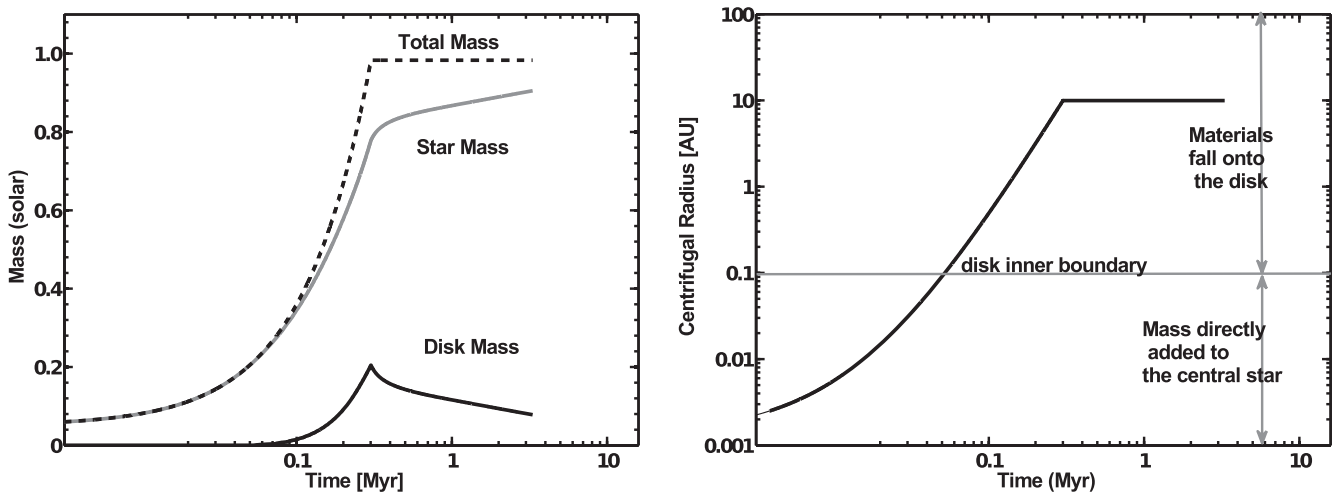

Fig. 2. Left panel shows the star mass, disk mass, and total system mass as a function of time. Within the first 0.3 Myr, both the star mass and disk mass grow. At 0.3 Myr, the star reached $\sim$0.8 $M_{\odot}$, and the disk reached $\sim$0.2 $M_{\odot}$. After infall stopped, the disk material gradually is accreted by the central star. Thus, the disk mass decreases, whereas the star mass increases. Right panel shows the centrifugal radius as a function of time.

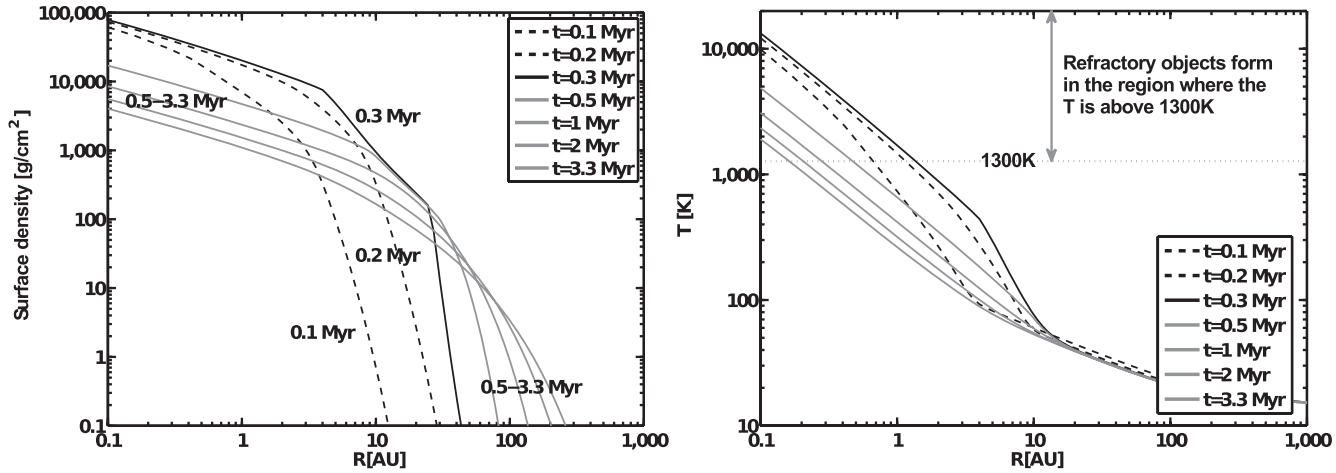

Fig. 3. The left panel shows the disk surface density versus orbital distance from the Sun at different times. The dashed black lines indicate the disk evolution during the infall stage. The black solid line represents the time when the collapse stopped. The gray lines show the disk profiles once infall has ceased. The right panel shows the disk midplane temperature profile at different times, with the lines being at the same times as those in the left figure. As can be seen, the temperature at the disk midplane increases during infall, especially in the region inside of 10 AU. Once infall has ceased, the disk cools over time.

A change in the slope in the surface density is seen in the region from approximately 5 AU to about 30 AU from 0.3 Myr to about 1 Myr. This is due to the increase of disk viscosity that develops as this region becomes gravitationally unstable, as shown in Fig. 4. That is, in this region, spiral arms would develop, which are able to increase the efficiency with which mass and angular momentum are transported (Armitage et al. 2001; Boss 2004, 2008). As a result, mass in the gravitationally unstable region, which is in the outer disk from a few astronomical units to tens of astronomical units, is redistributed much faster than that in the inner disk, explaining the discontinuity in the surface density distribution.

The temperature at the disk midplane increases during infall, as the increase in disk surface density leads to greater viscous dissipation and higher rates of heat production as well as greater optical depths, which thus trap the dissipated energy more effectively. This dissipated energy is only a significant source of heat inside of 10 AU. Farther out in the disk, the temperature structure is mainly determined by irradiation from the central star. Once infall has ceased, the disk cools over time, as viscous dissipation slows and the disk thins

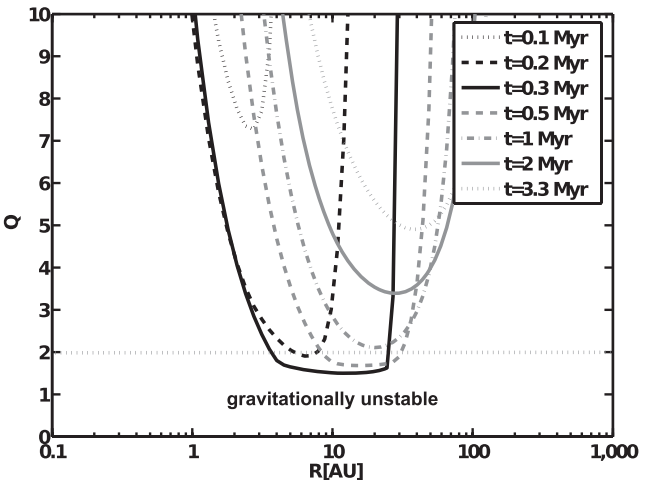

Fig. 4. The Q parameter distribution in the disk at different times. In the region where $Q < 2$, which is below the horizontal dashed line, the self-gravity of the disk exceeds the tidal force exerted by the central star, and thus this region becomes gravitationally unstable.

allowing the heat to be radiated away more effectively. It is in the above setting that we explore the formation and dynamic transport of high-temperature materials.

Applications to the Dynamics of Refractory Objects

Minerals found in most CAIs, such as corundum, hibonite, and spinel, are stable at $T > \sim$1300–1700 K in a solar nebula at 10^{-4}–10^{-3} bar total pressure (Grossman 1972, 2010; Davis and Richter 2005). Here, we track the dynamical evolution of "refractory objects" in our model. The total pressure at the midplane of the inner, hot region is in the 10^{-5}–10^{-1} bar range in our model. Thus, the exact temperature required to form CAIs would vary with locations in the disk. However, the temperature in the inner region changes so steeply that the difference between the location where $T > 1300$ K and where $T > 1700$ K is nearly identical in our model. Thus we define refractory objects, generally, as those materials which reached $T > 1300$ K in the hot, inner region of the disk. Note that this material could also represent Mg-rich silicates that condense from a vapor at roughly this temperature (Wooden et al. 2005). The high-temperature materials considered here could include those infalling materials that were incorporated into the disk in regions hotter than 1300 K, or those materials that were incorporated farther out, but then migrated within the disk to the hot regions. It can be seen in Fig. 3 that refractory objects would form in the disk out to approximately 2 AU at 0.3 Myr, the time when infall ceased. And after 3 Myr of disk evolution, the refractory objects can still form, but only inside 0.2 AU of the disk.

Following Ciesla (2010), we divide the refractory objects into different groups, depending on when they were exposed to $T > 1300$ K. We take the time when the particles last saw these high temperatures as the "formation age" and refer to it as such in our discussion. This formation age applies whether the particles saw these high temperatures only once during this time interval, or if the particles were part of an earlier generation that then migrated inwards to be exposed to the high temperatures again, thus they were recycled and made part of a younger population.

We have tracked the distribution of six different populations of refractory objects at 0.1 Myr intervals (those forming between 0 and 0.1 Myr, those forming between 0.1 and 0.2 Myr, and so on), with the final population being those that formed any time after 0.5 Myr. Here, we only consider fine-grained refractory objects whose dynamical behaviors are the same as that of gas (larger objects are considered further below). The left panel of Fig. 5 shows the fraction of different populations of refractory objects at a given location of the disk after 1 Myr of total evolution. As can be seen, those refractory objects continue to form and be added to the >0.5 Myr population even after 1 Myr of disk evolution ($\sim$0.7 Myr after infall ceased). This population is abundant in the inner, hot region, but its abundance drops rapidly farther away from the Sun. Those objects that formed earlier are more abundant in a vast majority of the disk. Refractory grains in the terrestrial planet region of the disk are dominated by those that formed during the final stages of infall, which is within 0.1–0.2 and 0.2–0.3 Myr in our model. The most abundant refractory grains in the outer regions (>10 AU) of the disk are those that formed within 0.1–0.2 Myr, with those formed at <0.1 Myr become increasingly dominant outside 100 AU, although this represents a small total mass at these extreme distances.

The earliest formed refractory grains dominate the extreme outer regions of the solar nebula because such grains are able to ride the early wave of the disk expansion. As such, the materials that are pushed farthest from the star are those that formed earliest.

In the 2–5 AU region of the disk, the populations from 0.1 to 0.2, 0.2 to 0.3, and 0.3 to 0.4 Myr dominate (make up $>90\%$) the high-temperature materials present after 1 Myr of solar nebula evolution, which are those populations nearest the time when infall ends. We subdivided these three populations into 0.05 Myr age intervals and repeated the calculation. The abundance of each population is shown in Fig. 6. Within these abundant populations, it is those objects formed immediately before infall ceased, that is 0.25–0.30 Myr in our model, that dominate in the 2–5 AU region. This is due to the combination of disk dynamics and the mass

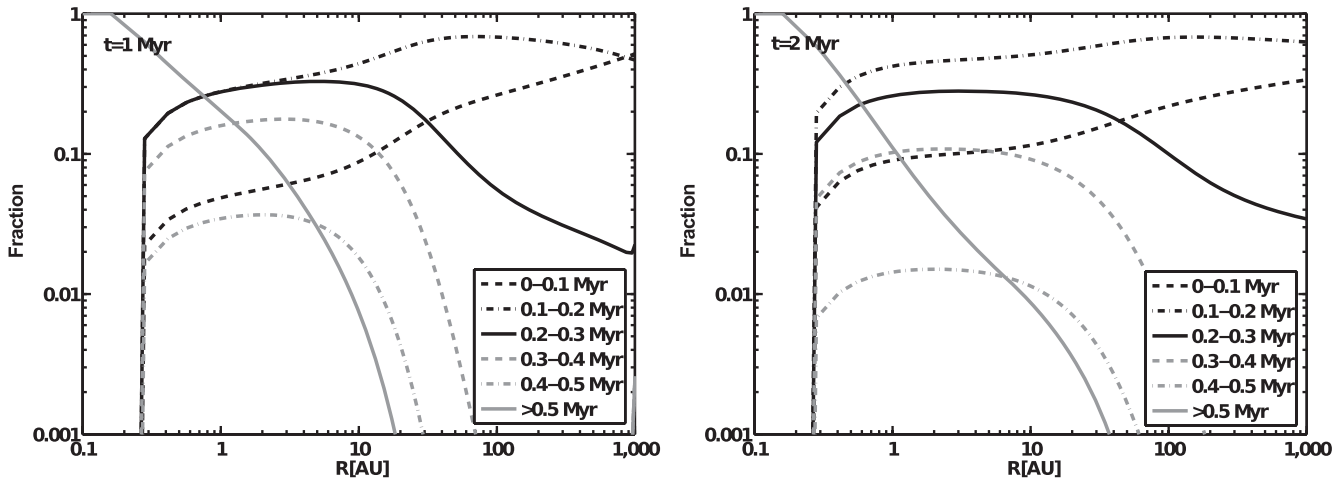

Fig. 5. Fractions of high-temperature materials that were formed within 0.1 Myr time intervals at different locations in the disk after 1 and 2 Myr of solar nebula evolution on the left and right, respectively. The black lines indicate those materials formed during the infall stage, whereas gray lines represent those high-temperature materials formed after infall ceased.

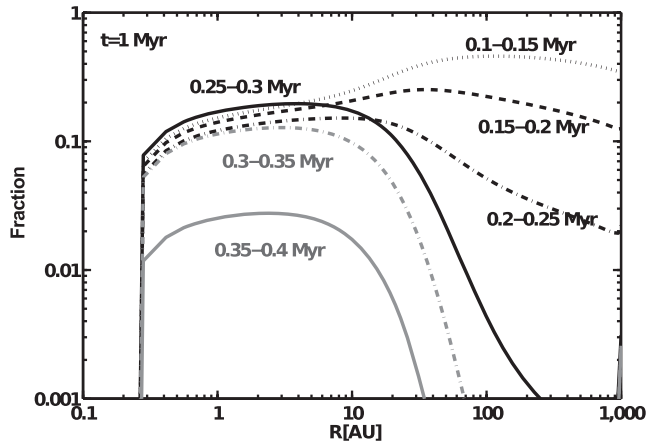

Fig. 6. Fractions of high-temperature materials that were formed within 0.05 Myr time intervals after 1 Myr of solar nebula evolution. The time intervals attached to the lines indicate each population's formation time, respectively.

distribution of the disk as described by Ciesla (2010). At those epochs, the disk goes through rapid radial expansion as mass from the infalling cloud is added preferentially to the inner regions of the disk, fueling the outward velocities. Further, the hot region of the disk contains the greatest amount of mass during these periods, which allows the greatest amount of refractory grains to be produced. Thus, while this population would be accreted into the central star along with inward gas flow just as other populations would be, in total number, grains from this population will still be more abundant than others.

After two millions of years, the relative abundance of each population changes slightly as shown in the right panel of Fig. 5. The most abundant population in the 2–5 AU region is now those grains from 0.1 to 0.2 Myr. The relative abundances of population from 0 to 0.1 Myr also become more abundant, which differs from the snapshot at 1 Myr. Thus, the high-temperature materials formed during the infall stage are relatively more abundant at 2 Myr than they were at 1 Myr of disk evolution. This is due to the fact that the net motions of disk materials in the inner tens of astronomical units are inwards at later times, meaning that the materials present in the inner disk then are more representative of the materials found in the outer disk during earlier times. Given that the populations from 0 to 0.1 and 0.1 to 0.2 Myr were more abundant in the outer disk ($R > 10$ AU) after 1 Myr, they become more abundant in the inner disk at these later times. As chondrite meteorite parent bodies formed 2 Myr or more after CAIs (Amelin et al. 2002, 2010; Krot et al. 2009), this result suggests that under the conditions assumed here, the refractory objects available in the region where these bodies would form (probably the 2–5 AU region) were those that formed immediately before or at the time that infall stopped. Later, we will return to discuss the implications of these results for interpreting the origins of meteoritic and cometary materials in detail.

Figure 7 shows the fraction of grains exposed to $T > 1300$ K throughout the disk, regardless of formation time, at different periods of nebular evolution. That is, the grains are found as two types: those that saw high temperatures and those that did not. These high temperatures are found inside of 2 AU throughout the evolution of the disk, and materials from this region get redistributed throughout the rest of the disk as described above. During the infall stage, the abundance of the high-

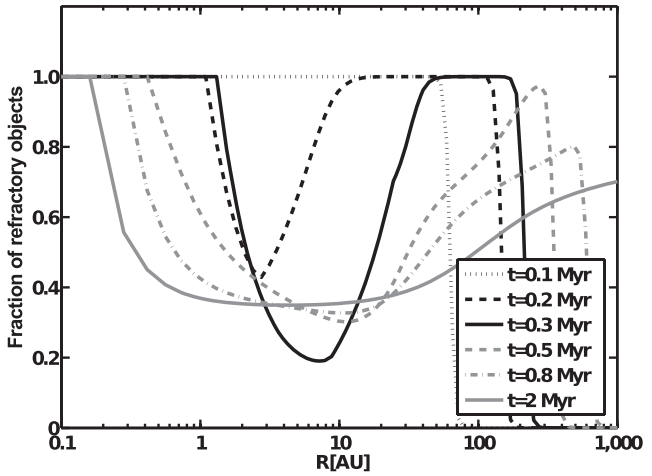

Fig. 7. The proportion of high-temperature materials in disk as a function of location (radius, R) at various epochs after the onset of collapse of the parent cloud. The vertical line in the outer region at each time is due to numerical treatment representing the spatial extent of the dust in the disk. As seen in the left panel of Fig. 3, the vertical lines coincide with the location where the surface density is very small.

temperature grains is diluted by the freshly added presolar, pristine grains in the cooler regions of the disk. That is the reason for the dips shown in the 0.2 and 0.3 Myr snapshots, when the molecular cloud materials are incorporated into the disk out to approximately 5 and approximately 10 AU, respectively. It is worth noting that despite this dilution, the fraction of high-temperature materials goes up at greater distances from the Sun at these time intervals. This is because viscous spreading has carried some high-temperature grains outwards to the distance where they cannot be immediately diluted by the freshly accreted materials (outside R_c). As such, the abundance of high-temperature materials is not monotonically decreasing away from the central star, and this nonmonotonic distribution persists even after millions of years of evolution within the disk. While the focus has been refractory inclusions as stated earlier, we can also consider this as a mechanism for the vaporization of amorphous precussors and the recondenstaion of crystalline grains. Similar spatial distributions of crystallinity were also predicted by Dullemond et al.'s (2006) model. This result runs counter to those models which begin with a fully formed disk and then allow high-temperature materials to diffuse outwards from the hot inner regions of the disk (Gail 2001; Bockelée-Morvan et al. 2002; Cuzzi et al. 2003; Ciesla 2007, 2009, 2010), and must be kept in mind when using the relative abundance of high-temperature materials to constrain mixing parameters for the solar nebula (e.g., Ogliore et al. 2009; Westphal et al. 2009).

These results may seem inconsistent with astronomical observations showing decreasing crys-tallinity with increasing radial distance in protoplanetary disks (Van Boekel et al. 2004; Min et al. 2005; Watson et al. 2009). However, their spatial resolution is such that the crystallinity is averaged over tens to hundreds of astronomical units, and would not see the fine spatial structure predicted in our model.

OTHER MODELS

We have described the results for our standard case in the previous section. Given that key parameters in this model are uncertain and expected to vary within a wide range of possible values, here we quantify how the model prediction would be impacted by changes in these parameters.

Variations with the Cloud's Initial Angular Momentum

In the standard case (model *a*), the initial angular velocity of parent cloud is set as 10^{-14} s^{-1}. The net effect of varying the initial angular velocity in our model is to alter the location where materials from the molecular cloud core are incorporated into the star–disk system (Fig. 8, right plot). That is, higher angular rotation rates would result in more angular momentum and thus materials falling further from the star at any given time. This would result in more massive and larger protoplanetary disks, whereas lower angular momentum would lead to less massive disks with steeper surface density profiles.

We have carried out two additional simulations with similar initial conditions as our standard case but with higher and lower angular rotation rates, respectively, and results are shown in Fig. 8. The centrifugal radius at the end of infall changes from 2.5 to 40 AU with the ω_{cd} varying from 5×10^{-15} to 2×10^{-14} s^{-1}. The fraction of high-temperature materials formed in different time intervals after 2 Myr disk evolution is plotted in Fig. 9, which can be compared to the right panel of Fig. 5 above.

In model *b* with the lower initial ω_{cd} as 5×10^{-15} s^{-1}, the cloud materials fall closer to the central star with a higher fraction of disk materials being exposed to $T > 1300$ K. However, the high-temperature materials that formed after infall stopped are less abundant than the standard case due to the lower mass of the disk. This lower amount of mass results in a cooler disk, which means temperatures in excess of 1300 K are confined to very close to the Sun, allowing only a small number of refractory grains to be produced at these later times. Thus, the dominant populations of high-temperature materials after 2 Myr disk evolution are those from 0.1 to 0.2 and

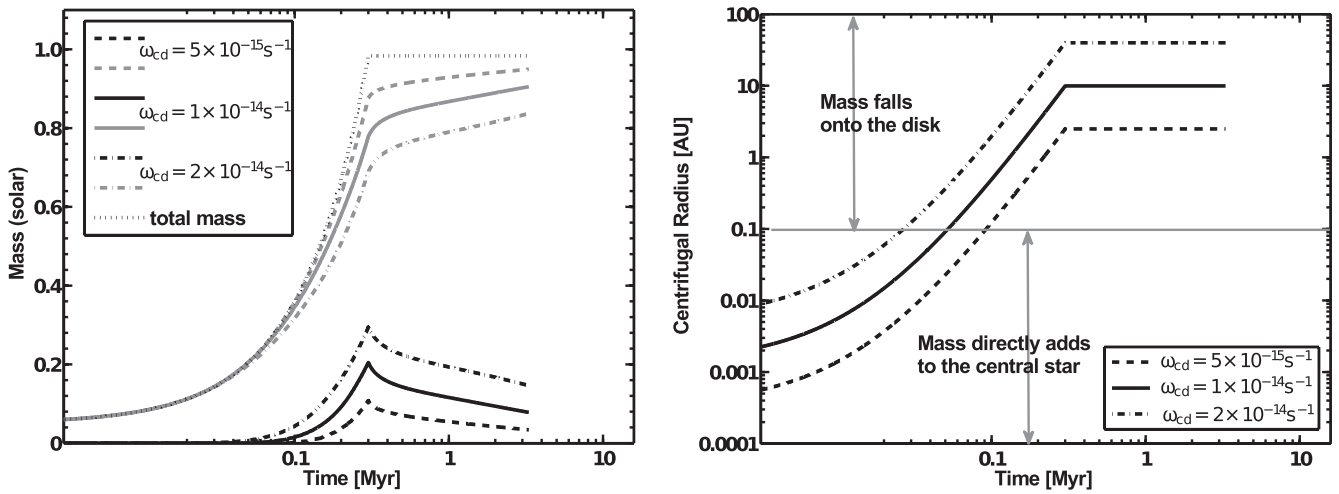

Fig. 8. The evolutions of star mass, disk mass, total system mass (left), and centrifugal radii (right) are shown. The initial angular velocity of each case varies as 5×10^{-15} s^{-1} (model *b*), 10^{-14} s^{-1} (model *a*), 2×10^{-14} s^{-1} (model *c*).

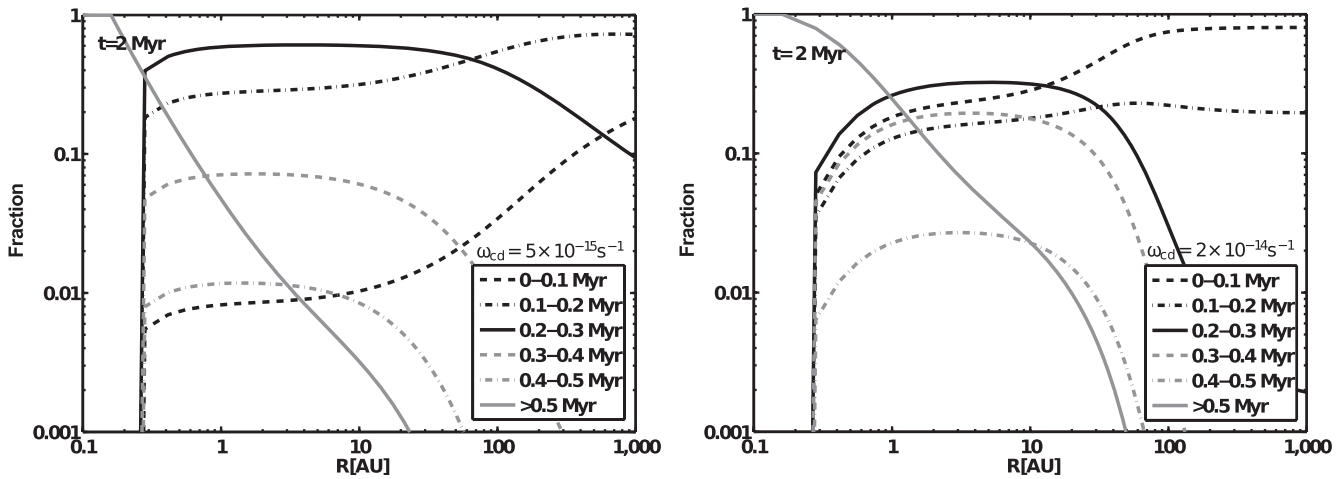

Fig. 9. The fraction of high-temperature materials that were formed and transported outwards within different time intervals after 2 Myr of solar nebula evolution in the cases in which the initial angular velocity are 5×10^{-15} s^{-1} (left figure, model *b*) and 2×10^{-14} s^{-1} (the right one, model *c*), respectively. The black lines indicate those materials formed during the infall stage, whereas gray lines represent those high-temperature material formed after infall ceased.

0.2 to 0.3 Myr. The reason for the low relative abundance of those formed between 0 and 0.1 Myr is that the disk receives mass only after 0.08 Myr as shown in Fig. 8.

In model *c* with the higher initial ω_{cd} as 2×10^{-14} s^{-1}, a lower fraction of material gets exposed to the high temperatures during infall as the centrifugal radius is larger in this case. This means that materials are added to the colder region of the disk at greater amounts. Because the disk in this situation is more massive, a larger fraction of high-temperature materials could still form after infall stopped, as shown in the right panel of Fig. 9. Another thing to note is that the population of refractory materials formed between 0 and 0.1 Myr is much more abundant than that in our standard case. This is due to two reasons. First, the centrifugal radius grows beyond 0.1 AU earlier than the standard case as shown in Fig. 8, and thus allows more refractory objects to form early and get transported outwards. Second, gravitational instabilities become more important in this more massive disk. The increased viscosities due to the spiral arms outside of 10 AU region will inhibit the outward expansion of materials from the relatively less active inner disk once the disk grows massive enough at later times. Therefore, the high-temperature materials formed in the first time interval that rode the wave of the disk expansion to the outer disk during earlier times can make up a considerable fraction of the materials in the 2–5 AU region.

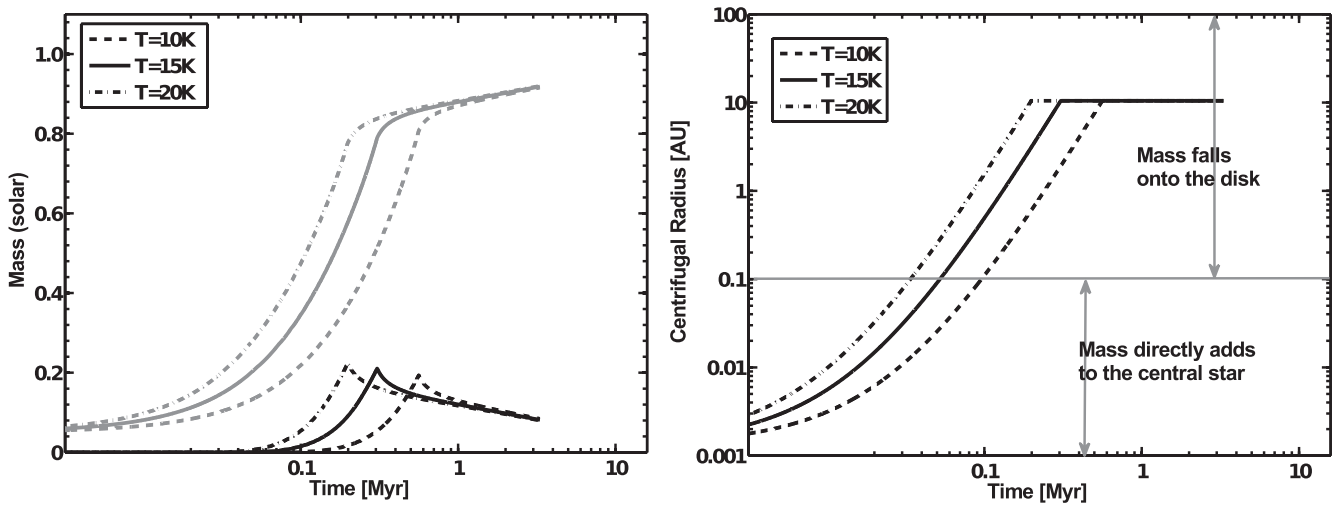

Fig. 10. The star mass and disk mass evolve as a function of time in cases where the cloud initial temperature varies as 10 K (model *d*), 15 K (model *a*), 20 K (model *e*). Infall stopped at 0.56, 0.30, and 0.20 Myr, respectively.

While there are differences in the details of the distributions that are attributed to the different dynamical evolution expected within these disks, two general trends remain: (1) grains in the outer regions of the disk are dominated by those that formed during the earliest stages of infall, and (2) grains that are most abundant in the inner regions of the disk (2–5 AU region) are those that formed right before or at the time when infall ceased. Thus, these chronology variations appear to be robust in terms of the initial angular momentum of the system.

Variations in the Initial Temperature of the Cloud Core

Another free parameter in our model is the molecular cloud temperature T_{cd}. Changes in this temperature affect our model in two ways. First, the expected radius of a collapsing core is $R_{cd} = GM/2c_s^2$. Thus, hotter cores would be smaller. If we keep the rotation rate constant, this would lead to a lower initial angular momentum as well. Thus, we also change the cloud's initial angular rotation rate such that the centrifugal radius of material in the outmost shell of the cloud is the same as that in the standard case. Second, the infall rate of mass from the core onto the star–disk system goes as $T_{cd}^{3/2}$, as described in Equation 1. Thus, hotter clouds collapse on shorter time scales, whereas cooler clouds do so on longer time scales. These effects are shown in Fig. 10. The infall time, t_{infall}, for 10 K (model *d*) and 20 K (model *e*) clouds are thus 0.56 and 0.20 Myr, respectively.

Figure 11 again shows the distribution of the different age populations throughout the two disks 2 Myr after infall began. In each case, a total of six age populations were tracked as in our standard case, with the duration of time that each population represents being determined by the infall time of the parent cloud core ($\Delta t \sim t_{infall}/3$). Comparing Fig. 11 with the right panel of Fig. 5, there are only slightly differences, although the most abundant population in the 2–5 AU region are still those that formed right before the time that infall ceased. Further, the oldest population of high-temperature grains continues to dominate those in the outer disk.

Variations with Anomalous Viscosity

Here, we investigate the effects of varying the α parameter on the distributions of high-temperature materials. The α parameter determines the magnitude of viscosity in our model, which will determine the mass and angular momentum transport in the disk.

First, we set the basic α parameter as 10^{-5} and leave all other parameters unchanged from the standard case. This low value is approximately what would be expected in the Dead Zone of a disk (Fleming and Stone 2003). In this situation (model *f*), the disk undergoes significant dynamical evolution only in the gravitationally unstable region as spiral arms form and locally increase the effective α. That is the reason for the sharp decrease of gas surface density at the edge of disk as shown in left panel of Fig. 12.

As shown in Fig. 12, the most abundant high-temperature material in the outer disk after 2 Myr is material formed during the 0.1–0.2 Myr interval. As the disk is much more massive, high temperatures are maintained for a longer period of time, allowing those materials formed after infall ended to dominate the population of high-temperature materials in the 2–5 AU region. However, due to the lower level of transport, the relative proportion of each population changes over very

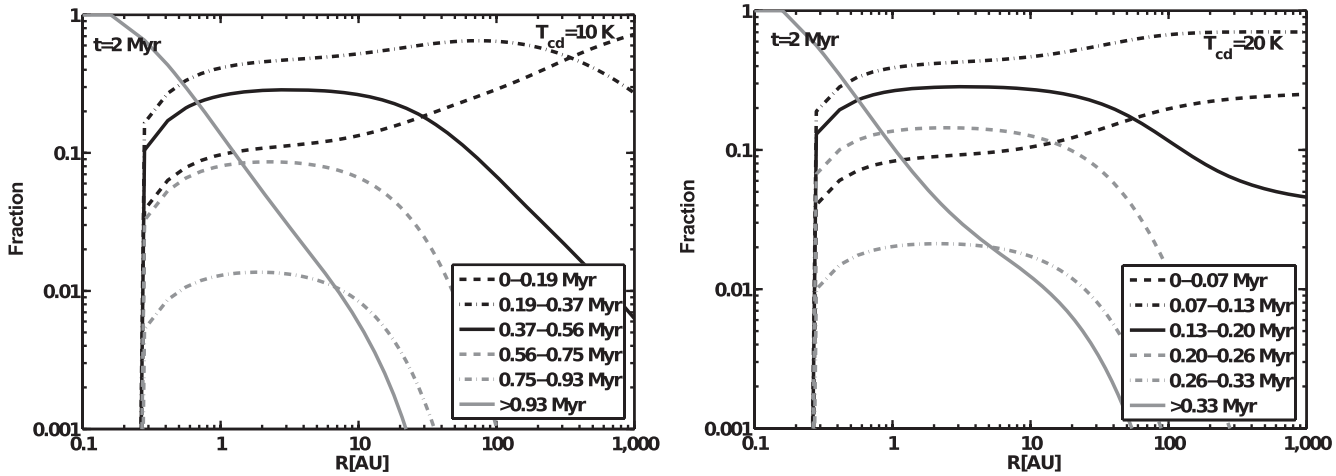

Fig. 11. The fraction of high-temperature materials that were formed and transported outwards within different time intervals after 2 Myr of solar nebula evolution in the cases where the initial temperatures are 10 K (left figure, model *d*) and 20 K (right figure, model *e*). Black lines indicate those materials formed during the infall stage, whereas gray lines represent those high-temperature materials formed after infall ceased.

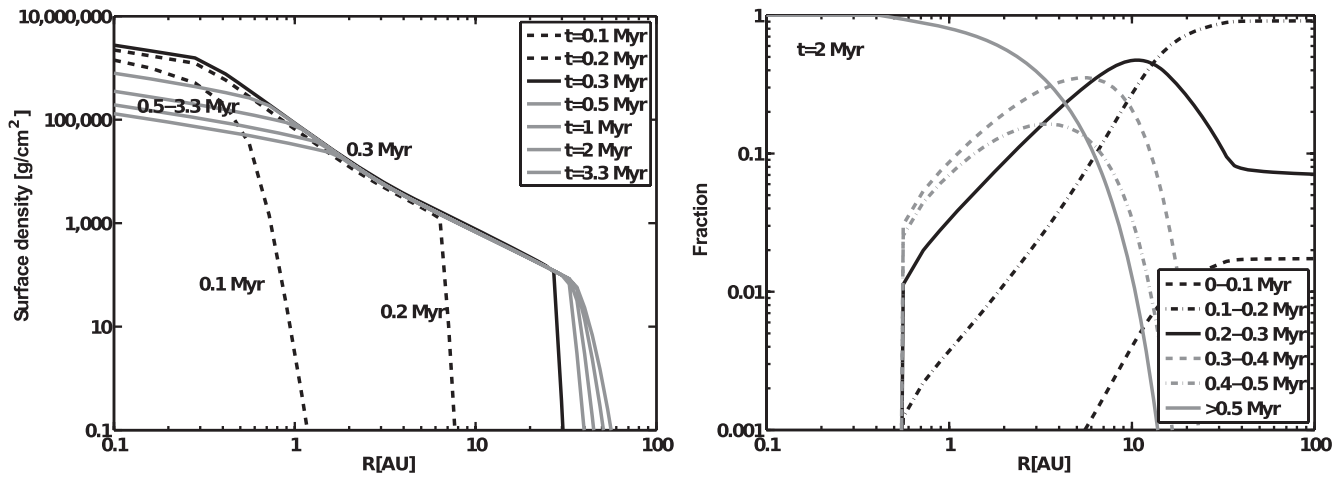

Fig. 12. The left figure shows the disk surface density versus orbital distance at different times in the case that the viscosity is essentially only due to gravitational instabilities (model *f*). The right figure is a snapshot of the fraction of high-temperature materials that were formed and transported outwards within different time intervals after 2 Myr of solar nebula evolution in the case of $\alpha = 10^{-5}$.

small spatial scales. As a result, a collection of refractory objects from the inner disk would probably exhibit greater scatter in terms of ages than in the cases described above, which would be dominated by those from a particular time interval.

We also consider a situation in which α varies spatially in the disk (model *g*). The goal of this approach is to account for variations that may arise due to disk evolution being controlled by the magnetorotational instability (MRI; Balbus and Hawley 1991). That is, the MRI occurs only in regions of the disk where the gas is sufficiently ionized. In the region where gas is not ionized enough and thus decoupled from the magnetic field, the viscosity can be relatively small (orders of magnitude smaller) compared to the MRI active region where the turbulence α parameter describing viscosity can reach 0.001–0.1 (Papaloizou and Nelson 2003). The dominant source of ionization in a disk is likely cosmic rays and X-rays (Gammie 1996; Glassgold et al. 1997), which penetrate only a finite depth into the disk. This would mean that the midplane of the dense, inner region of the disk was likely evolving much more slowly than the sparse, outer regions where cosmic rays and X-rays were able to penetrate all the way down to the disk midplane.

To perform a first-order examination of the spatial variation of viscosity on the redistribution of high-

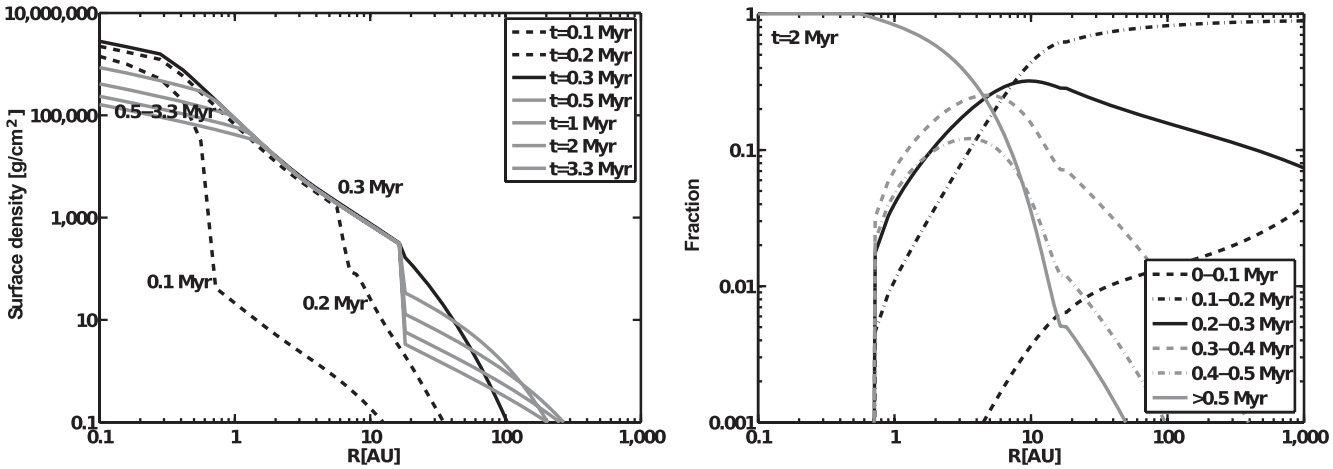

Fig. 13. The left panel shows the disk surface density versus orbital distance at different times in the case that the viscosity varies along with the surface density (model *g*). In the region where the surface density is higher than 200 g cm^{-2}, the basic α is set as 10^{-5}, and in the region where surface density is lower than 200 g cm^{-2}, the basic α is chosen to be 10^{-2}. Here, the molecular cloud initial angular velocity is 10^{-14} s^{-1}. The right figure is a snapshot of the fraction of high-temperature materials that were formed and transported outwards within different time intervals; after 2 Myr of solar nebula evolution in this case.

temperature materials, we allowed α to be a function of the surface density of gas. If the gas surface density is below $\Sigma_{\rm crit}$, we assume that cosmic rays or X-rays are able to penetrate to the disk midplane and fully ionize the column of gas. Here, we adopt $\Sigma_{\rm crit} = 200$ g cm^{-2} (which is 100 g cm^{-2} on each side of the disk midplane) and set the basic $\alpha = 10^{-2}$ in the active region and $\alpha = 10^{-5}$ in the rest of the disk. A similar approach is adopted in planet formation models of Matsumura et al. (2009).

As can be seen from Fig. 13, gas is effectively transported in the outer region since the surface density there is low enough for the MRI to be active, and is held up in the inner region due to the weak viscous transport. The viscosity in the inner region is largely due to gravitational instabilities, as the typical viscosity is so low with our choice of α. As a result, the distributions of high-temperature material formed at different times in the disk after 2 Myr of evolution change compared to the standard case. Specifically, the dominant refractory objects at 2–5 AU are those formed after 0.5 Myr. On the other hand, those materials in the outer disk are still dominated by those objects that formed well before infall ceased.

Variations with the Opacity

The opacity in a given region of the disk is determined by the amount of dust present, its temperature, its size distribution, and its composition. In the cases considered thus far, we set the opacity of disk material, κ, as 1 cm^2 g^{-1} throughout the whole disk, which is a typical value for cosmic mixture of gas and fine dust in protoplanetary disks (Cassen 2001). To examine the effect of the assumed opacity in our study, we also consider a case where the opacity varies with disk properties (model *h*).

As dust is the dominant source of opacity, we decrease the opacity to 0.0001 cm^2 g^{-1} where a large fraction of it would be vaporized ($T > 1300$ K), and assume a value of 5 cm^2 g^{-1} where it has condensed ($T < 1300$ K). In those regions where it is vaporized, it is likely only vaporized around the disk midplane due to the vertical temperature gradient in the disk. Thus, a linear combination of 5 and 0.0001 cm^2 g^{-1} is used in this region, unless the effective temperature is so high that dust would also be absent at all heights. Then a total opacity of 0.0001 cm^2 g^{-1} is adopted. This treatment of opacity is similar to those used in Cassen (1994) and Ciesla (2010).

The thermal structure of solar nebula is shown in the left panel of Fig. 14, which can be compared with the right panel of Fig. 3. The midplane temperature generally decreases with increase in distance away from the central star in the disk. However, an isothermal region with temperature approximately at the dust condensation temperature exists in the disk between approximately 0.2 and 3 AU. That is because pure gas exists in the midplane there covered by dust layers, and the midplane temperature is close to temperature at the dust condensation front due to the small opacity of gas. As a result, the region where refractory objects can form still stretches out to 0.6 AU even after 2 Myr of disk evolution, compared with 0.2 AU in the standard case. This is because the lower temperature in these regions early in disk evolution leads to slower, more prolonged mass transport.

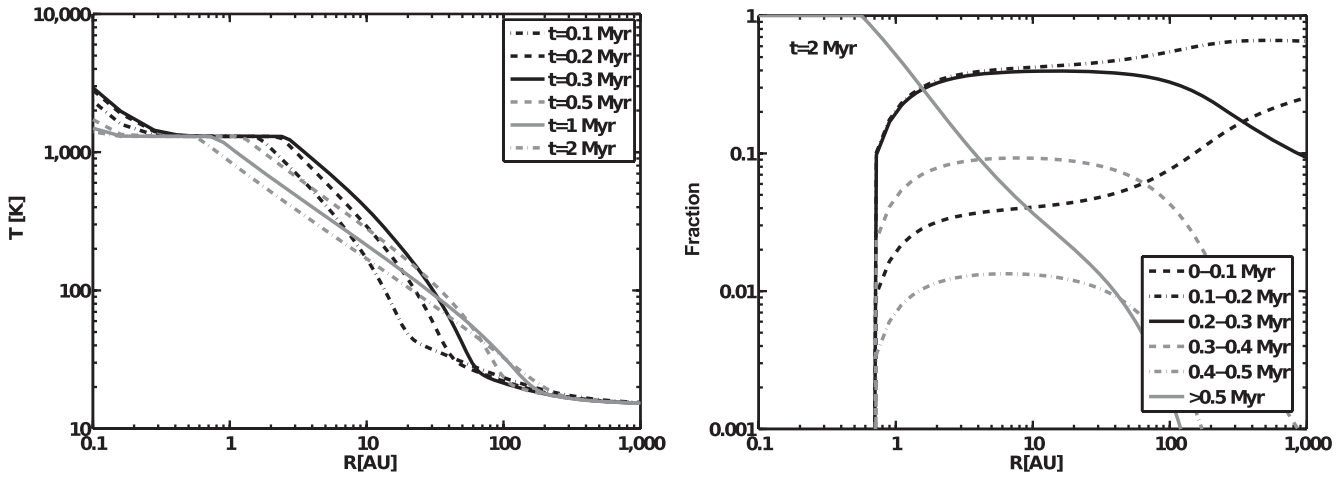

Fig. 14. The left panel shows the disk midplane temperature versus orbital distance at different times in the case that the opacity varies (model *h*). The treatment of opacity variation is described in the text. The right panel is the snapshot of the fraction of high-temperature materials that were formed and transported outwards within different time intervals after 2 Myr of solar nebula evolution.

The distributions of high-temperature materials formed in different time intervals after 2 Myr evolution are shown in the right panel of Fig. 14. It can be seen that, although the disk thermal structure changes, varying the values of opacity does not significantly alter the relative abundances of each population from what were seen above.

Variations of Grain Size

Until now, we have focused on fine-grained dust being redistributed through the disk. However, some CAIs, particularly those found in the CV chondrites, are in the millimeter- to centimeter-size range. They would be strongly affected by gas drag, causing them to spiral inwards, toward the central star. As such, in our 1-D radial mixing model, those materials would constantly be pushed back inwards due to this effect.

To understand how the inward drift impacted the distribution of high-temperature materials in the disk, we performed a run for particles large enough to be affected by gas drag. Here, we introduce a parameter, the nondimensional stopping time, τ_s, which is the ratio of the time scale for a particle to lose its relative velocity with respect to the gas to its dynamical time, or the time for it to orbit the central star. The value of τ_s determines how strongly gas drag influences transport of the particle (Weidenschilling 1977; Cuzzi et al. 1993; Takeuchi and Lin 2002; Cuzzi and Weidenschilling 2006).

$$\tau_s = \frac{r_s \rho_s}{\rho_g C_S} \Omega, \tag{9}$$

where r_s is the particle radius, ρ_s is the particle internal density and is set as 1g cm^{-3}, and ρ_g is local gas density and is calculated as the midplane density in our 1-D model $\rho_g = \Sigma/(\sqrt{2\pi}H)$. Thus, τ_s can be written as $(\sqrt{2\pi} r_s \rho_s)/\Sigma$, meaning that τ_s generally increases with a decrease in disk surface density, and thus with increasing distance from the central star. In this consideration, we set $r_s = 0.1$cm.

The particle radial migration rate is described as (Takeuchi and Lin 2002)

$$\upsilon_p = \frac{\tau_s^{-1}\upsilon_r}{\tau_s + \tau_s^{-1}} - \frac{\eta R \Omega}{\tau_s + \tau_s^{-1}}, \tag{10}$$

where $\eta = -(1/R\Omega^2\rho_g)(\partial P_g/\partial R)$ is the ratio of the radial pressure gradient in the nebular gas to the central force of gravity from the central star. The first term on the right hand side of Equation 10 accounts for the radial motions associated with flow of the gas, and the second term is due to gas drag.

Here, the dynamical behavior of 1 mm size particles is described by Equation 8 except substituting υ_r with υ_p and $D = \nu/(1+\tau_s^2)$ (Youdin and Lithwick 2007). Further, when those particles enter regions of the nebula with $T > 1700$ K, they will evaporate locally, with the vapor species moving as gas. Here, the distance that those particles drift in the hot region before evaporating (Cuzzi et al. 2003) is ignored. The left panel of Fig. 15 shows the normalized fraction of high-temperature materials—the ratio of the surface densities of the refractory objects to the gas, divided by their expected abundance in a gas of solar composition. An enhancement of refractory materials within their evaporation front is shown in that plot, which is caused by the different dynamical behavior of the particles outside the evaporation front and the vapor inside (e.g., Cuzzi and Zahnle 2004; Ciesla and Cuzzi 2006).

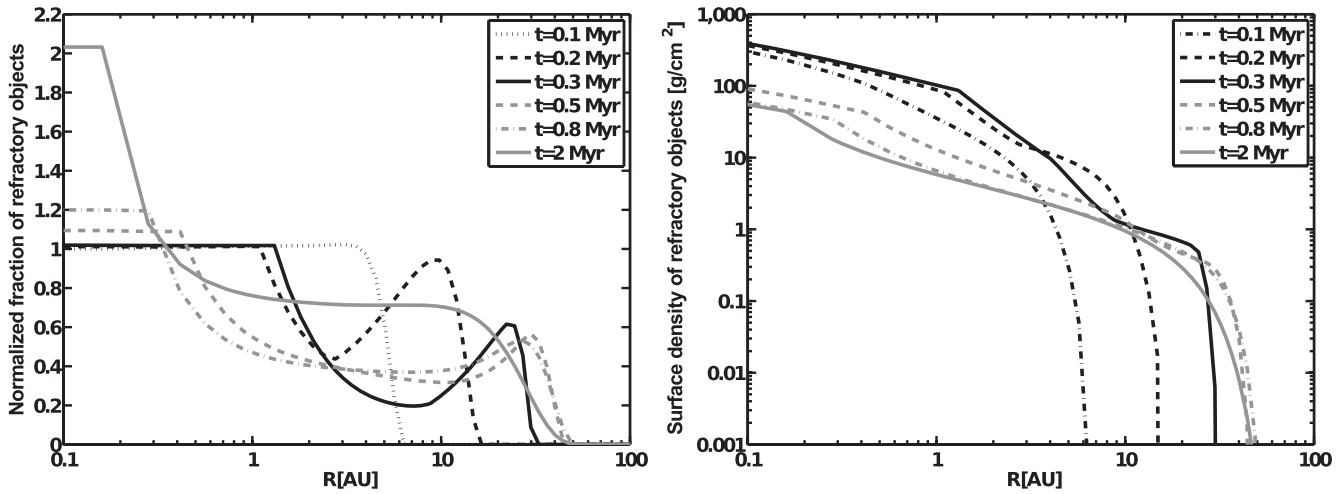

Fig. 15. Left panel shows the normalized fractions of high-temperature materials as a function of location (radius, R) at various epochs after the onset of collapse of the parent cloud are shown. The normalized fraction is calculated as the ratio of the surface densities of the refractory objects to the gas, divided by the dust to gas ratio expected in a gas of solar composition (5×10^{-3}). Right panel shows the high-T material surface density versus orbital distance at different times.

In the early evolution of the disk, the rapid radial expansion it underwent allowed for even the larger particles considered here to be pushed to the cooler, outer regions of the disk. That is, the outward velocities associated with the evolution of the disk (the first term on the right side of Equation 10) were sufficient to offset the inward motions of particles due to gas drag (second term). This was particularly true during infall, as molecular cloud material was added to the disk at small distances, generating surface density gradients that supported net outward movement throughout much of the disk.

After infall stops, gas drag becomes more important relative to the outward velocities of the disk. This leads to particles drifting inwards and beginning to experience the classic problem of "spiraling inward to the Sun." As shown in Fig. 15, however, while particles drift inward with time, their normalized abundance after 2 Myr remains at $>20\%$ the value expected for a gas of solar composition. This means that if CAI-like materials made up approximately 5% of the mass of condensables in this region (Cuzzi et al. 2003), then CAIs would make up at least 1% of the mass of those forming at this time in the disk. In the 2–5 AU region where chondrite parent bodies might form, we estimate approximately 1–3% of the mass of a given chondrite would be composed of these larger objects, which compares favorably to the abundances reported for carbonaceous chondrites (Scott 2007).

This differs from those findings from Cuzzi et al. (2003) and Ciesla (2010) who saw much greater drops in the abundance of these large particles over the same time period. The outward velocities of the gas in the models presented here are generally larger than in previous studies, allowing particles to migrate farther out in the disk, and thus have longer lifetimes in the disk as they must travel greater distances to be lost to the Sun. This is similar to the very rapid expansion predicted by Jacquet et al. (2011) due to the greater activity predicted in the early phase of the evolution of the solar nebula, which gives way to more gradual inward drift of the particles. That the overall abundances of the large CAIs is greater in our models than previous models is significant, as it suggests that should the CAIs form in a manner consistent with what we outline here, the formation and natural evolution of the disk would provide the dynamic conditions which would allow their preservation, with little to no need of enhancements of solid-forming species in the CAI factory (Cuzzi et al. 2003) or significant preferential settling of the larger objects (Ciesla 2010).

Figure 16 shows that, although all high-temperature materials are confined to be within approximately 60 AU in the disk by gas drag, those objects that formed during the infall stage still dominate the outer disk, and moreover dominate throughout the whole disk except the innermost hot region. Although gas drag works to limit the outward movement of all refractory objects, those early-formed objects were carried outwards with the wave of disk expansion. Thus, it is these objects which have the longest residence time in the disk and thus are available for accretion into parent bodies at later times. Thus, the dominant populations in the 2–5 AU region are still those formed between 0.1 and 0.2 Myr, with those forming between 0.2–0.3 and 0–0.1 Myr also being abundant.

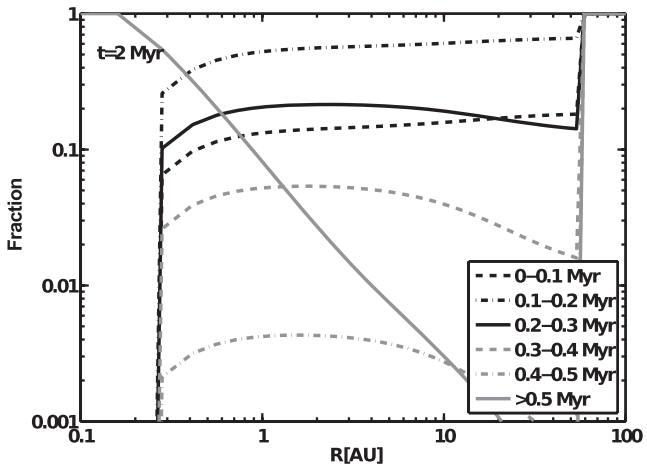

Fig. 16. Fractions of refractory materials that were formed within 0.1 Myr time intervals at different locations in the disk after 2 Myr of solar nebula evolution. The vertical line in the outer region (~60 AU) is due to numerical treatment representing the spatial extent of the dust in the disk. As seen in the right panel of Fig. 15, the vertical line coincides with the location where the surface density of refractory material is very small.

DISCUSSION

This study focused on the production and redistribution of high-temperature materials that formed in the hot ($T > 1300$ K) inner region of the solar nebula at different times of its evolution. Despite a number of uncertainties in the initial state of the cloud from which our solar system formed, our main results are found to be robust even when considering variations in key parameters in our model. In each case, those high-temperature materials formed during the molecular core collapse stage dominate the outer region of disk, while those materials formed later, around the time that infall stopped, are the most abundant population in the 2–5 AU region. Those materials formed well after infall stopped are only abundant in the inner, hot region of disk. These results suggest that at the time when chondritic meteorite parent bodies formed (>2 Myr in the nebular evolution), the refractory objects available for them to accrete were those that formed around the time that infall stopped.

Wood (2004) attempted to infer the astrophysical setting of CAI formation by comparing the observed spread in their ages to the duration of different stages of star and protoplanetary disk evolution. At that time, CAIs were thought to have formed over a period of approximately 0.5 Myr based on $^{26}Al/^{27}Al$ studies. Wood (2004) concluded that CAIs must have formed during parent cloud collapse, as this stage occurred on time scales of a few hundred thousand years (Feigelson and Montmerle 1999). In recent years, improved analyses have led the estimated duration of CAI formation to be reduced to approximately 10^4 yr (Thrane et al. 2006; Jacobsen et al. 2008). If we followed the arguments of Wood (2004), this would point to CAI forming during the initial stages of collapse (the class 0) as this is roughly the length of time this stage lasts. However, as Ciesla (2010) pointed out, CAI formation may actually have lasted for an extended time period, but due to the dynamical evolution of materials within a disk, the record we see in meteorites is biased toward a particular formation period. Our calculations support this conclusion, as we find those refractory materials that are present in the inner disk after >2 Myr of evolution are dominated by a particular period in time, that time right before the solar nebula stopped accreting mass from its parent cloud. This was found to be true in a large number of models, despite the fact that such high-temperature materials can form for millions of years within the disk.

These results allow us to better understand the astrophysical setting of CAI formation and the meaning of $t = 0$ in solar system chronology. While refractory materials may have formed for millions of years, those we find in meteorites will be dominated by the population that formed around the time that infall stopped. This likely would coincide with the transition from class I to class II stage of young stellar objects. There may be some refractory materials that formed both before and after this time; however, it is within that short time interval that most CAIs we observe today likely formed, and thus this would be $t = 0$ in solar system chronology.

Further, our model shows that the CAIs formed during the earliest stage of infall dominate the outer solar nebula. Thus, comets may contain high-temperature materials that formed during this time period. This allows us to re-interpret the age of Coki, a CAI-like object collected from comet Wild 2 by The Stardust mission that had subcanonical $^{26}Al/^{27}Al$ ratio at the time it formed (Matzel et al. 2010). It was originally interpreted that Coki formed in the inner solar system at least 1.7 Myr after the oldest CAIs so much of the canonical ^{26}Al would have decayed away. However, according to our model, as Coki was collected from a body which accreted in the outer solar nebula, it was likely among those high-temperature grains formed before infall ceased. It may thus have formed before ^{26}Al was introduced to the CAI formation region. This could be achieved if ^{26}Al was added to the molecular cloud core shortly before collapse (e.g., Gaidos et al. 2009) or as the triggering event for its collapse (Boss et al. 2008). If live ^{26}Al was among the later infalling materials from the parent cloud, those materials which formed before infall was complete would

contain little or no ^{26}Al. It is these materials that we predict to be present in the comet formation region. However, once the ^{26}Al was introduced into the CAI formation region, it would have to have been quickly homogenized in that region in order to be consistent with the uniform canonical abundance seen in chondritic meteorites (MacPherson et al. 1995; MacPherson 2005; Jacobsen et al. 2008) and the agreement in ^{26}Al ages and Pb-Pb ages (Amelin et al. 2002, 2010).

Moreover, our model could also help explain other observed isotopic heterogeneities among refractory inclusions in meteorites. For example, a range of ^{50}Ti excesses from average solar value is observed in CAIs (Leya et al. 2009). Clayton et al. (1988) reported that CAIs that record little or no live ^{26}Al show a much greater level of scatter in ^{50}Ti composition than those with canonical $(^{26}Al/^{27}Al)_0 \sim 5 \times 10^{-5}$. The correlation between $(^{26}Al/^{27}Al)_0$ and ^{50}Ti anomalies is also observed from studies of hibonites from Murchison chondrite (Ireland 1988; Liu et al. 2009). According to our model, these observations could be explained by isotopic heterogeneities existing during infall, but the disk becoming well mixed with time. Thus, those CAIs with high ^{50}Ti anomalies and little or no live ^{26}Al would have formed earlier as they preserve a heterogeneous distribution of ^{50}Ti in the parent cloud, and those CAIs with the lower anomalies formed afterwards when the ^{50}Ti got (partially) homogenized in the protoplanetary disk. Sahijpal and Goswami (1998) proposed a similar hypothesis, suggesting that those refractory phases showing no live ^{26}Al represent the first solar system solids. Our model supports this proposal and furthermore provides a theoretical framework in which this can occur. Similar arguments suggest that the FUN (Fractionation and Unidentified Nuclear isotope anomalies) CAIs (Wasserburg et al. 1977), which show little or no excess of ^{26}Mg from the decay of ^{26}Al (MacPherson 2005), would probably also be the earliest CAIs, which is also suggested by Wood (2004). What is needed to further explore this issue is a study that provides detailed statistics on the abundance of FUN CAIs or CAIs which did not have live ^{26}Al that can be compared to our model predictions.

There are other models that aim to explain the formation of high-temperature materials and transport in the solar nebula that we have not considered here. The X-wind model (Shu et al. 1996, 2001) proposed that CAIs formed very close to the Sun, were launched upwards by strong winds, and then fell back onto the disk at different locations. In addition, Wurm and Haack (2009) proposed that photophoresis drove CAIs outwards along the surface of protoplanetary disks very early on during high luminosity events, like FU-Orionis outbursts (Herbig 1977; Hartmann and Kenyon 1996). In the case of the X-wind model, objections have been raised about whether the predictions it makes are consistent with the chemistry and mineralogy of the objects in our solar system (Krot et al. 2009; Desch et al. 2010). We propose that another test for all transport models is determining whether the predicted age distributions of materials in the solar system are consistent with their observed ages.

While this study provides insight into the formation and redistribution of high-temperature materials in the solar nebula, there are issues that require further attention in developing our understanding of the origin of the solar system. First, our model of disk formation is based on Shu's (1977) model that the molecular cloud core undergoes inside-out collapse with a constant infall rate. This treatment neglects the roles of magnetic fields, supersonic turbulence, and rotation in the cloud, which would generally make the infall rate larger than that of Shu's (1977) model (McKee and Ostriker 2007). Further, the infall rate may not always be a constant during cloud collapse (e.g., Foster and Chevalier 1993; Schmeja and Klessen 2004). Those factors can complicate the simple picture used here, but likely would not change that the disk reaches the greatest amount of mass nearest the time when infall ends. Thus, the greatest amount of refractory grains still could form in the hot region around the time of greatest outward expansion and largest disk mass, and those age populations can dominate the high-temperature materials present in the 2–5 AU regions after a few million years.

Second, our model predicts a high abundance of high-temperature materials, like crystalline grains, in the outer disk, which is similar to the result of Dullemond et al. (2006). However, Visser and Dullemond (2010) thought that this was due to the idealized treatment of infalling material incorporated into the disk. In a 2-D frame (radius + vertical directions), trajectories of infalling material will intersect with the disk on the surface of the outer disk, rather than go directly to the midplane. Thus, a lower crystalline fraction in the outer disk is expected as lower fraction of materials is able to see high temperature of the inner region and refractories in the outer region are diluted by fresh cloud material. However, this consideration would not likely change the age distribution of refractory objects in the outer disk, which is the most abundant population that would have formed early and prior to the time when infall stopped. This is because the greatest amount of radial spreading, which is key in preserving these larger objects, will occur when material is added close to the Sun. If material is added far from the Sun, this will slow down the outward transport, and thus make preservation of all objects, more difficult.

Particle growth and fragmentation are also neglected in our model. As particles grow, their interactions with

the gas evolve, including developing an inward drift due to gas drag (e.g., Weidenschilling 1977). This could offset the outward motions of high-temperature grains or cause the first generation of particles to get locked up into planetesimals early in solar system history. On the other hand, particle fragmentation through high-speed collisions could replenish small grains in the disk (Dullemond and Dominik 2005). Both of these processes will change the dust size distribution in the disk spatially and temporally. However, these effects are likely more important during later stages of evolution when the disk evolution has slowed. For example, particle growth is likely inefficient beyond a few centimeters, as well as in regions of high turbulence, as might be expected during the formation and early evolution of the solar nebula (Blum 2010). Nonetheless, given that CAIs seen in various chondrites have different sizes (MacPherson 2005), these two processes would impact these populations differently, and thus are interesting issues that warrant further exploration.

Another aspect is that the disk in our model remains relatively massive after a few million years of evolution ($\sim$0.1 $M_\odot$). However, gas appears to be removed within a few million years (Simon and Prato 1995; Wolk and Walter 1996; Haisch et al. 2001). Photoevaporation could be a process responsible for disk gas removal, which we do not consider here. Photoevaporation occurs where the sound speed of photoionized gas exceeds the local gravitational escape speed, allowing gas to be lost from the disk surface. However, photoevaporation becomes important in shaping the structure of the disk once the mass accretion rate through the disk drops below $\sim 10^{-9}$ $M_\odot$ yr^{-1}, which has not yet occurred in the models we have presented here. Nonetheless, if a population of small particles remains in the disk at the later times when photoevaporation becomes important, its effects on the dust distribution should be considered (Alexander and Armitage 2007).

Based on the above discussion, it is unlikely that these considerations would drastically change our conclusions. Thus, it appears that the CAIs and other refractory materials we see today, which originated in the hot, inner region of the disk, mostly formed at about the time when the solar nebula stopped accreting material from its parent cloud core. This helps us understand the meaning of time zero of our solar system, which is from chronologic study of CAIs. Further we expect a significant population of refractory materials that formed before infall was complete to be preserved in primitive bodies, particularly in the outer disk.

Acknowledgments—We thank the referees, Stu Weidenschilling and Conel Alexander, for their excellent comments that helped improve the manuscript. We also thank Robert Clayton, Frank Richter, Andrew Davis, and Nicolas Dauphas for their helpful discussion and comments to improve the original manuscript. Funding for this work for both L. Y. and F. J. C. was provided by NASA grants NNX08AY47G and NNX11AK52G.

Editorial Handling—Dr. Edward Scott

REFERENCES

Adams F. C., Lada C. J., and Shu F. H. 1988. The disks of T Tauri stars with flat infrared spectra. *The Astrophysical Journal* 326:865–883.

Alexander R. D. and Armitage P. J. 2007. Dust dynamics during protoplanetary disc clearing. *Monthly Notices of the Royal Astronomical Society* 375:500–512.

Amelin Y., Krot A. N., Hutcheon I. D., and Ulyanov A. A. 2002. Lead isotopic ages of chondrules and calcium-aluminum-rich inclusions. *Science* 297:1678–1683.

Amelin Y., Kaltenbach A., Iizuka T., Stirling C. H., Ireland T. R., Petaev M., and Jacobsen S. B. 2010. U-Pb chronology of the solar system's oldest solids with variable $^{238}U/^{235}U$. *Earth and Planetary Science Letters* 300:343–350.

Armitage P. J., Livio M., and Pringle J. E. 2001. Episodic accretion in magnetically layered protoplanetary discs. *Monthly Notices of the Royal Astronomical Society* 324:705–711.

Balbus S. A. and Hawley J. F. 1991. A powerful local shear instability in weakly magnetized disks. I—Linear analysis. II—Nonlinear evolution. *The Astrophysical Journal* 376:214–233.

Barranco J. A. and Goodman A. A. 1998. Coherent dense cores. I. NH_3 observations. *The Astrophysical Journal* 504:207–222.

Blum J. 2010. Dust growth in protoplanetary disks—A comprehensive experimental/theoretical approach. *Research in Astronomy and Astrophysics* 10:1199–1214.

Bockelée-Morvan D., Gautier D., Hersant F., Huré J., and Robert F. 2002. Turbulent radial mixing in the solar nebula as the source of crystalline silicates in comets. *Astronomy & Astrophysics* 384:1107–1118.

Boss A. P. 2004. Evolution of the solar nebula. VI. Mixing and transport of isotopic heterogeneity. *The Astrophysical Journal* 616:1265–1277.

Boss A. P. 2008. Mixing in the solar nebula: Implications for isotopic heterogeneity and large-scale transport of refractory grains. *Earth and Planetary Science Letters* 268:102–109.

Boss A. P., Ipatov S. I., Keiser S. A., Myhill E. A., and Vanhala H. A. T. 2008. Simultaneous triggered collapse of the presolar dense cloud core and injection of short-lived radioisotopes by a supernova shock wave. *The Astrophysical Journal* 686:L119–L122.

Brownlee D., Tsou P., Aléon J., Alexander C. M. O'. D., Araki T., Bajt S., Baratta G. A., Bastien R., Bland P., Bleuet P., Borg J., Bradley J. P., Brearley A., Brenker F., Brennan S., Bridges J. C., Browning N. D., Brucato J. R., Bullock E., Burchell M. J., Busemann H., Butterworth A., Chaussidon M., Cheuvront A., Chi M., Cintala M. J., Clark B. C., Clemett S. J., Cody G., Colangeli L., Cooper G., Cordier P., Daghlian C., Dai Z., D'Hendecourt L., Djouadi Z., Dominguez G., Duxbury T., Dworkin J. P., Ebel D. S.,

Economou T. E., Fakra S., Fairey S. A. J., Fallon S., Ferrini G., Ferroir T., Fleckenstein H., Floss C., Flynn G., Franchi I. A., Fries M., Gainsforth Z., Gallien J.-P., Genge M., Gilles M. K., Gillet P., Gilmour J., Glavin D. P., Gounelle M., Grady M. M., Graham G. A., Grant P. G., Green S. F., Grossemy F., Grossman L., Grossman J. N., Guan Y., Hagiya K., Harvey R., Heck P., Herzog G. F., Hoppe P., Hörz F., Huth J., Hutcheon I. D., Ignatyev K., Ishii H., Ito M., Jacob D., Jacobsen C., Jacobsen S., Jones S., Joswiak D., Jurewicz A., Kearsley A. T., Keller L. P., Khodja H., Kilcoyne A. L. D., Kissel J., Krot A., Langenhorst F., Lanzirotti A., Le L., Leshin L. A., Leitner J., Lemelle L., Leroux H., Liu M., Luening K., Lyon I., MacPherson G., Marcus M. A., Marhas K., Marty B., Matrajt G., McKeegan K., Meibom A., Mennella V., Messenger K., Messenger S., Mikouchi T., Mostefaoui S., Nakamura T., Nakano T., Newville M., Nittler L. R., Ohnishi I., Ohsumi K., Okudaira K., Papanastassiou D. A., Palma R., Palumbo M. E., Pepin R. O., Perkins D., Perronnet M., Pianetta P., Rao W., Rietmeijer F. J. M., Robert F., Rost D., Rotundi A., Ryan R., Sandford S. A., Schwandt C. S., See T. H., Schlutter D., Sheffield-Parker J., Simionovici A., Simon S., Sitnitsky I., Snead C. J., Spencer M. K., Stadermann F. J., Steele A., Stephan T., Stroud R., Susini J., Sutton S. R., Suzuki Y., Taheri M., Taylor S., Teslich N., Tomeoka K., Tomioka N., Toppani A., Trigo-Rodríguez J. M., Troadec D., Tsuchiyama A., Tuzzolino A. J., Tyliszczak T., Uesugi K., Velbel M., Vellenga J., Vicenzi E., Vincze L., Warren J., Weber I., Weisberg M., Westphal A. J., Wirick S., Wooden D., Wopenka B., Wozniakiewicz P., Wright I., Yabuta H., Yano H., Young E. D., Zare R. N., Zega T., Ziegler K., Zimmerman L., Zinner E., and Zolensky M. 2006. Comet 81P/Wild 2 under a microscope. *Science* 314:1711–1716.

Cassen P. 1994. Utilitarian models of the solar nebula. *Icarus* 112:405–429.

Cassen P. 2001. Nebular thermal evolution and the properties of primitive planetary materials. *Meteoritics & Planetary Science* 36:671–700.

Ciesla F. J. 2007. Outward transport of high-temperature materials around the midplane of the solar nebula. *Science* 318:613–615.

Ciesla F. J. 2009. Two-dimensional transport of solids in viscous protoplanetary disks. *Icarus* 200:655–671.

Ciesla F. J. 2010. The distributions and ages of refractory objects in the solar nebula. *Icarus* 208:455–467.

Ciesla F. J. and Cuzzi J. N. 2006. The evolution of the water distribution in a viscous protoplanetary disk. *Icarus* 181:178–204.

Clayton R. N., Hinton R. W., and Davis A. M. 1988. Isotopic variations in the rock-forming elements in meteorites. *Philosophical Transactions of the Royal Society of London* 325:483–501.

Cuzzi J. N. and Weidenschilling S. J. 2006. Particle-gas dynamics and primary accretion. In *Meteorites and the early solar system II*, edited by Lauretta D. S. and McSween J. H. Y. Tucson, Arizona: The University of Arizona Press. pp. 353–381.

Cuzzi J. N. and Zahnle K. J. 2004. Material enhancement in protoplanetary nebulae by particle drift through evaporation fronts. *The Astrophysical Journal* 614:490–496.

Cuzzi J. N., Dobrovolskis A. R., and Champney J. M. 1993. Particle-gas dynamics in the midplane of a protoplanetary nebula. *Icarus* 106:102–134.

Cuzzi J. N., Davis S. S., and Dobrovolskis A. R. 2003. Blowing in the wind. II. Creation and redistribution of refractory inclusions in a turbulent protoplanetary nebula. *Icarus* 166:385–402.

Davis A. M. and Richter F. M. 2005. Condensation and evaporation of solar system materials. In *Meteorites, comets and planets: Treatise on geochemistry, vol. 1*, edited by Davis A. M. Oxford: Elsevier-Pergamon. pp. 407–430.

Desch S. J., Morris M. A., Connolly H. C., and Boss A. P. 2010. A critical examination of the X-wind model for chondrule and calcium-rich, aluminum-rich inclusion formation and radionuclide production. *The Astrophysical Journal* 725:692–711.

Dullemond C. P. and Dominik C. 2005. Dust coagulation in protoplanetary disks: A rapid depletion of small grains. *Astronomy & Astrophysics* 434:971–986.

Dullemond C. P., Apai D., and Walch S. 2006. Crystalline silicates as a probe of disk formation history. *The Astrophysical Journal* 640:L67–L70.

Feigelson E. D. and Montmerle T. 1999. High-energy processes in young stellar objects. *Annual Review of Astronomy and Astrophysics* 37:363–408.

Fleming T. and Stone J. M. 2003. Local magnetohydrodynamic models of layered accretion disks. *The Astrophysical Journal* 585:908–920.

Foster P. N. and Chevalier R. A. 1993. Gravitational collapse of an isothermal sphere. *The Astrophysical Journal* 416:303–311.

Gaidos E., Krot A. N., Williams J. P., and Raymond S. N. 2009. ^{26}Al and the formation of the solar system from a molecular cloud contaminated by Wolf-Rayet winds. *The Astrophysical Journal* 696:1854–1863.

Gail H.-P. 2001. Radial mixing in protoplanetary accretion disks. I. stationary disc models with annealing and carbon combustion. *Astronomy & Astrophysics* 378:192–213.

Gammie C. F. 1996. Layered accretion in T Tauri disks. *The Astrophysical Journal* 457:355–362.

Glassgold A. E., Najita J., and Igea J. 1997a. X-ray ionization of protoplanetary disks. *The Astrophysical Journal* 480:344–350.

Glassgold A. E., Najita J., and Igea J. 1997b. X-ray ionization of protoplanetary disks: Erratum. *The Astrophysical Journal* 485:920.

Goodman A. A., Benson P. J., Fuller G. A., and Myers P. C. 1993. Dense cores in dark clouds. VIII—Velocity gradients. *The Astrophysical Journal* 406:528–547.

Grossman L. 1972. Condensation in the primitive solar nebula. *Geochimica et Cosmochimica Acta* 36:597–619.

Grossman L. 2010. Vapor-condensed phase processes in the early solar system. *Meteoritics & Planetary Science* 45:7–20.

Haisch K. E. Jr., Lada E. A., and Lada C. J. 2001. Disk frequencies and lifetimes in young clusters. *The Astrophysical Journal* 553:L153–L156.

Harker D. E., Wooden D. H., Woodward C. E., and Lisse C. M. 2002. Grain properties of comet C/1995 O1 (Hale-Bopp). *The Astrophysical Journal* 580:579–597.

Harker D. E., Wooden D. H., Woodward C. E., and Lisse C. M. 2004a. Erratum: "Grain properties of comet C/1995 O1 (Hale-Bopp)" (*ApJ*, 580, 579 [2002]). *The Astrophysical Journal* 615:1081.

Harker D. E., Woodward C. E., Wooden D. H., and Kelley M. S. 2004b. The dust mineralogy of two long-period comets: C/2001 Q4 (neat) and C/2002 T7 (linear). American

Astronomical Society Meeting 205, #56.12. *Bulletin of the American Astronomical Society* 36:1434.

Hartmann L. and Kenyon S. J. 1996. The FU Orionis phenomenon. *Annual Review of Astronomy and Astrophysics* 34:207–240.

Hartmann L., Calvet N., Gullbring E., and D'Alessio P. 1998. Accretion and the evolution of T Tauri disks. *The Astrophysical Journal* 495:385–410.

Herbig G. H. 1977. Eruptive phenomena in early stellar evolution. *The Astrophysical Journal* 217:693–715.

Hueso R. and Guillot T. 2005. Evolution of protoplanetary disks: Constraints from DM Tauri and GM Aurigae. *Astronomy & Astrophysics* 442:703–725.

Ireland T. R. 1988. Correlated morphological, chemical, and isotopic characteristics of hibonites from the Murchison carbonaceous chondrite. *Geochimica et Cosmochimica Acta* 52:2827–2839.

Jacobsen B., Yin Q., Moynier F., Amelin Y., Krot A. N., Nagashima K., Hutcheon I. D., and Palme H. 2008. ^{26}Al-^{26}Mg and ^{207}Pb-^{206}Pb systematics of Allende CAIs: Canonical solar initial ^{26}Al/^{27}Al ratio reinstated. *Earth and Planetary Science Letters* 272:353–364.

Jacquet E., Fromang S., and Gounelle M. 2011. Radial transport of refractory inclusions and their preservation in the dead zone. *Astronomy & Astrophysics* 526:L8.

Kemper F., Vriend W. J., and Tielens A. G. G. M. 2004. The absence of crystalline silicates in the diffuse interstellar medium. *The Astrophysical Journal* 609:826–837.

Krot A. N., Amelin Y., Bland P., Ciesla F. J., Connelly J., Davis A. M., Huss G. R., Hutcheon I. D., Makide K., Nagashima K., Nyquist L. E., Russell S. S., Scott E. R. D., Thrane K., Yurimoto H., and Yin Q.-Z. 2009. Origin and chronology of chondritic components: A review. *Geochimica et Cosmochimica Acta* 73:4963–4997.

Lada C. J. and Wilking B. A. 1984. The nature of the embedded population in the Rho Ophiuchi dark cloud—Mid-infrared observations. *The Astrophysical Journal* 287:610–621.

Lada C. J. and Shu F. H. 1990. The formation of sunlike stars. *Science* 248:564–572.

Leya I., Schönbächler M., Krähenbühl U., and Halliday A. N. 2009. New titanium isotope data for Allende and Efremovka CAIs. *The Astrophysical Journal* 702:1118–1126.

Lisse C. M., VanCleve J., Adams A. C., A'Hearn M. F., Fernández Y. R., Farnham T. L., Armus L., Grillmair C. J., Ingalls J., Belton M. J. S., Groussin O., McFadden L. A., Meech K. J., Schultz P. H., Clark B. C., Feaga L. M., and Sunshine J. M. 2006. Spitzer spectral observations of the deep impact ejecta. *Science* 313:635–640.

Liu M., McKeegan K. D., Goswami J. N., Marhas K. K., Sahijpal S., Ireland T. R., and Davis A. M. 2009. Isotopic records in CM hibonites: Implications for timescales of mixing of isotope reservoirs in the solar nebula. *Geochimica et Cosmochimica Acta* 73:5051–5079.

Lodato G. 2008. Classical disc physics. *New Astronomy Review* 52:21–41.

Lodders K. 2003. Solar system abundances and condensation temperatures of the elements. *The Astrophysical Journal* 591:1220–1247.

Lynden-Bell D. and Pringle J. E. 1974. The evolution of viscous discs and the origin of the nebular variables. *Monthly Notices of the Royal Astronomical Society* 168:603–637.

MacPherson G. J. 2005. Calcium-aluminum-rich inclusions in chondritic meteorites. In *Meteorites, comets and planet: Treatise on geochemistry, vol. 1*, edited by Davis A. M. Oxford: Elsevier–Pergamon. pp. 201–246.

MacPherson G. J., Davis A. M., and Zinner E. K. 1995. The distribution of aluminum-26 in the early solar system—A reappraisal. *Meteoritics* 30:365–386.

Matsumura S., Pudritz R. E., and Thommes E. W. 2009. The growth and migration of Jovian planets in evolving protostellar disks with dead zones. *The Astrophysical Journal* 691:1764–1779.

Matzel J. E. P., Ishii H. A., Joswiak D., Hutcheon I. D., Bradley J. P., Brownlee D., Weber P. K., Teslich N., Matrajt G., McKeegan K. D., and MacPherson G. J. 2010. Constraints on the formation age of cometary material from the NASA Stardust mission. *Science* 328: 483–486.

McKee C. F. and Ostriker E. C. 2007. Theory of star formation. *Annual Review of Astronomy and Astrophysics* 45:565–687.

McKeegan K., Aléon J., Bradley J., Brownlee D., Busemann H., Butterworth A., Chaussidon M., Fallon S., Floss C., Gilmour J., Gounelle M., Graham G., Guan Y., Heck P., Hoppe P., Hutcheon I., Huth J., Ishii H., Ito M., Jacobsen S., Kearsley A., Leshin L., Liu M., Lyon I., Marhas K., Marty B., Matrajt G., Meibom A., Messenger S., Mostefaoui S., Mukhopadhyay S., Nakamura-Messenger K., Nittler L., Palma R., Pepin R., Papanastassiou D., Robert F., Schlutter D., Snead C., Stadermann F., Stroud R., Tsou P., Westphal A., Young E., Ziegler K., Zimmermann L., and Zinner E. 2006. Isotopic compositions of cometary matter returned by Stardust. *Science* 314:1724–1728.

Min M., Hovenier J. W., de Koter A., Waters L. B. F. M., and Dominik C. 2005. The composition and size distribution of the dust in the coma of comet Hale Bopp. *Icarus* 179:158–173.

Nakamoto T. and Nakagawa Y. 1994. Formation, early evolution, and gravitational stability of protoplanetary disks. *The Astrophysical Journal* 421:640–650.

Ogliore R. C., Westphal A. J., Gainsforth Z., Butterworth A. L., Fakra S. C., and Marcus M. A. 2009. Nebular mixing constrained by the Stardust samples. *Meteoritics & Planetary Science* 44:1675–1681.

Papaloizou J. C. B. and Nelson R. P. 2003. The interaction of a giant planet with a disc with MHD turbulence—I. The initial turbulent disc models. *Monthly Notices of the Royal Astronomical Society* 339:983–992.

Pollack J. B., McKay C. P., and Christofferson B. M. 1985. A calculation of the rosseland mean opacity of dust grains in primordial solar system nebulae. *Icarus* 64:471–492.

Ruden S. P. and Pollack J. B. 1991. The dynamical evolution of the protosolar nebula. *The Astrophysical Journal* 375:740–760.

Sahijpal S. and Goswami J. N. 1998. Refractory phases in primitive meteorites devoid of ^{26}Al and ^{41}Ca: Representative samples of first solar system solids? *The Astrophysical Journal* 509:L137–L140.

Schmeja S. and Klessen R. S. 2004. Protostellar mass accretion rates from gravoturbulent fragmentation. *Astronomy & Astrophysics* 419:405–417.

Scott E. R. D. 2007. Chondrites and the protoplanetary disk. *Annual Review of Earth and Planetary Sciences* 35:577–620.

Shakura N. I. and Sunyaev R. A. 1973. Black holes in binary systems. Observational appearance. *Astronomy & Astrophysics* 24:337–355.

Shu F. H. 1977. Self-similar collapse of isothermal spheres and star formation. *The Astrophysical Journal* 214:488–497.

Shu F. H., Shang H., and Lee T. 1996. Toward an astrophysical theory of chondrites. *Science* 271:1545–1552.

Shu F. H., Shang H., Gounelle M., Glassgold A. E., and Lee T. 2001. The origin of chondrules and refractory inclusions in chondritic meteorites. *The Astrophysical Journal* 548:1029–1050.

Simon M. and Prato L. 1995. Disk dissipation in single and binary young star systems in Taurus. *The Astrophysical Journal* 450:824–829.

Takeuchi T. and Lin D. N. C. 2002. Radial flow of dust particles in accretion disks. *The Astrophysical Journal* 581:1344–1355.

Thrane K., Bizzarro M., and Baker J. A. 2006. Extremely brief formation interval for refractory inclusions and uniform distribution of ^{26}Al in the early solar system. *The Astrophysical Journal* 646:L159–L162.

Toomre A. 1964. On the gravitational stability of a disk of stars. *The Astrophysical Journal* 139:1217–1238.

Van Boekel R., Min M., Leinert C., Waters L. B. F. M., Richichi A., Chesneau O., Dominik C., Jaffe W., Dutrey A., Graser U., Henning T., de Jong J., Köhler R., de Koter A., Lopez B., Malbet F., Morel S., Paresce F., Perrin G., Preibisch T., Przygodda F., Schöller M., and Wittkowski M. 2004. The building blocks of planets within the ''terrestrial'' region of protoplanetary disks. *Nature* 432:479–482.

Van Dishoeck E. F., Blake G. A., Draine B. T., and Lunine J. I. 1993. The chemical evolution of protostellar and protoplanetary matter. In *Protostars and planets III*, edited by Levy E. H. and Lunnine J. Tucson, Arizona: University of Arizona Press. pp. 163–241.

Visser R. and Dullemond C. P. 2010. Sub-Keplerian accretion onto circumstellar disks. *Astronomy & Astrophysics* 519:A28.

Wasserburg G. J., Lee T., and Papanastassiou D. A. 1977. Correlated O and Mg isotopic anomalies in Allende inclusions. II—Magnesium. *Geophysical Research Letters* 4:299–302.

Watson D. M., Leisenring J. M., Furlan E., Bohac C. J., Sargent B., Forrest W. J., Calvet N., Hartmann L., Nordhaus J. T., Green J. D., Kim K. H., Sloan G. C., Chen C. H., Keller L. D., d'Alessio P., Najita J., Uchida K. I., and Houck J. R. 2009. Crystalline silicates and dust processing in the protoplanetary disks of the Taurus young cluster. *The Astrophysical Journal Supplement Series* 180:84–101.

Weidenschilling S. J. 1977. Aerodynamics of solid bodies in the solar nebula. *Monthly Notices of the Royal Astronomical Society* 180:57–70.

Westphal A. J., Fakra S. C., Gainsforth Z., Marcus M. A., Ogliore R. C., and Butterworth A. L. 2009. Mixing fraction of inner solar system material in comet 81P/Wild2. *The Astrophysical Journal* 694:18–28.

Wolk S. J. and Walter F. M. 1996. A search for protoplanetary disks around naked T Tauri stars. *The Astronomical Journal* 111:2066–2076.

Wood J. A. 2004. Formation of chondritic refractory inclusions: The astrophysical setting. *Geochimica et Cosmochimica Acta* 68:4007–4021.

Wooden D. H., Harker D. E., and Brearley A. J. 2005. Thermal processing and radial mixing of dust: Evidence from comets and primitive chondrites. In *Chondrites and the protoplanetary disk*, ASP Conference Series, vol. 341, Proceedings of a workshop held 8-11 November 2004 in Kaua'i, Hawai'i, edited by Krot A. N., Scott E. R. D., and Reipurth B. San Francisco: Astronomical Society of the Pacific. pp. 774–808.

Wurm G. and Haack H. 2009. Outward transport of CAIs during FU-Orionis events. *Meteoritics & Planetary Science* 44:689–699.

Youdin A. N. and Lithwick Y. 2007. Particle stirring in turbulent gas disks: Including orbital oscillations. *Icarus* 192:588–604.

Young J. S. and Scoville N. Z. 1991. Molecular gas in galaxies. *Annual Review of Astronomy and Astrophysics* 29:581–625.

Zhu Z., Hartmann L., and Gammie C. 2010. Long-term evolution of protostellar and protoplanetary disks. II. Layered accretion with infall. *The Astrophysical Journal* 713:1143–1158.